Hyperspectral Remote Sensing of Conifer Biochemistry in the Greater Victoria Watershed District, British Columbia

by

Sarah Elizabeth Alice McDonald
B.E.S., University of Waterloo, 2001

A Thesis Submitted in Partial Fulfillment of the
Requirements for the Degree of

MASTER OF SCIENCE

in the Department of Geography

Supervisor: Dr. K.O. Niemann

ABSTRACT

The biochemical composition of conifer foliage in the Greater Victoria Watershed District (GVWD), Vancouver Island, Canada, was examined using hyperspectral remote sensing data. Imagery acquired from the airborne sensor Advanced Visible/Infrared Imaging Spectrometer (AVIRIS) was compared to sampled foliar chemical measurements to provide regional maps of biochemical distribution. The biochemical concentrations of nitrogen, chlorophyll and moisture derived from AVIRIS data were analyzed to provide an analysis of the forest canopy, comprised predominantly of Douglas-fir.

The AVIRIS data were preprocessed to correct for atmospheric and geometric distortion, degradation, and noise inherent in the data in order to properly represent the forest canopy at the time of image acquisition. The AVIRIS data were used to investigate the relationship between the reflectance, absorbance and derivative values present in the imagery corresponding to the sampled chemical data. A total of 29 plots were used in a partial least squares regression analysis to analyze the relationship between the data sets to extract chemical constituents in the forest canopy. Nitrogen and total chlorophyll models have r^2 values of 0.73 and 0.68 respectively. Due to the complexity of moisture interaction with hyperspectral data, regression models were unable to be computed for the AVIRIS data over the GVWD. Regression models were then applied to the entire AVIRIS dataset for regional mapping of the canopy

biochemistry. The distribution of nitrogen and total chlorophyll in the forested areas of the GVWD was mapped.

TABLE OF CONTENTS

LIST OF TABLES

ACKNOWLEDGMENTS

I would like to thank Dr. Olaf Niemann for his guidance and support while working on this thesis. Dr. David Goodenough, at the Pacific Forestry Centre, for providing the AVIRIS and ancillary data as well as valuable insight into the use of hyperspectral remote sensing in forestry applications. Andrew Dyk and the Advanced Forest Technologies team at PFC for their technical expertise in image processing techniques.

Lastly, I would like to thank my family for their never-ending encouragement in completing my thesis and for giving me the drive and determination for knowledge.

To Stephen F. McDonald and Sharon McBride,
My parents;

and Isabel Robertson,
My grandmother.

1.0 INTRODUCTION AND RESEARCH OBJECTIVES

Canada contains 10% of the world's forests; therefore it is necessary to monitor and sustain this natural resource for future generations. The health and continuity of forest resources is of great environmental and economic benefit to the country. Forests are essential to moderate climate, filter air and water and provide a habitat for terrestrial life. Not only are forests important environmentally, but also economically the industry generates $34 billion dollars toward Canada's trade surplus, employs 353,000 people and provides the basis for a $2 billion dollar tourism industry in Canada (Natural Resources Canada, 2002). On an annual basis approximately 0.4% (1 million hectares) of the 417 million hectares of boreal and temperate forests are harvested and 1.6% of forests are affected by fire, insects and disease (Canadian Forest Service, 2002). Therefore it is imperative to evaluate and monitor Canada's forests as a sustainable resource for future generations. Research is ongoing in federal and provincial government, academia and the private sector to ensure the sustainability of Canada's forests.

Historically, aerial surveys have been used to provide inventory attributes of Canada's forests. However, due to the financial constraints and the need for expertise in processing the data, a more cost-effective method of obtaining forest attributes was required. Consequently, with the launch of the spaceborne multispectral sensor Landsat-1 in 1972, a method of acquiring forest information over a large area at one time became feasible for use in forest management practices. This technology provided the ability to map forest cover, monitor resource depletion and measure biophysical properties of Canada's forests (Canada Centre for Remote Sensing, 2003). With the development of space-based Radio

Detection And Range (RADAR) sensors coupled with optical multispectral data, the ability to delineate areas of deforestation and assess soil conditions for forest regeneration was achieved (Moran *et al.*, 2000). Recent advances in remote sensing technologies have provided a method of acquiring high spectral resolution data from airborne and spaceborne platforms. The ability to detect detailed forest attribute data using hyperspectral remote sensing has made it possible to examine forest health and species identification in detail.

With hyperspectral airborne and spaceborne sensors, such as Compact Airborne Spectrometer Imager (*casi)*, Advanced Visible/Infrared Imaging Spectrometer (AVIRIS) and Hyperion, detailed forest attributes can be examined. Hyperspectral sensors provide high signal to noise ratios, more spectral bands and greater radiometric resolution, which allows for identification of forest species and the monitoring of forest health (Curran *et al.*, 1997). Hyperspectral remote sensing, also known as imaging spectrometry, provides the ability to acquire a continuous spectrum of electromagnetic energy, in the visible and infrared regions, representing features on the Earth's surface (Lillesand and Kiefer, 1994). An analysis of this spectral response provides the ability to identify materials present in the imaged area, leading to the assessment of vegetation quality and abundance from a platform above the Earth's surface (Curran, 1989).

Monitoring the health of Canada's forests requires an understanding of ecosystem processes such as photosynthesis, nutrient cycling and net primary productivity. Hyperspectral remote sensing can be used to observe these processes and provide forest

canopy biochemistry estimates (Martin and Aber, 1997). Forest biochemistry, such as nitrogen, chlorophyll and moisture derived by imaging spectrometers, can be used to detect stress, assess vegetation quality and estimate the amount of new and old foliage (Gausman and Quisenberry, 1990). Understanding biochemical processes occurring in the forest canopy can lead to determining sources of stress in a forest ecosystem, such as disease and insect infestation, to provide an analysis of the health of Canada's forests

Understanding the distribution of foliar biochemistry in the forest canopy of the Greater Victoria Watershed District (GVWD) using hyperspectral remote sensing data can provide insight into ecological processes occurring in this region. During the growing seasons of 2000 and 2001, airborne hyperspectral data and foliar chemical samples were collected by the Pacific Forestry Centre (PFC), Natural Resources Canada (NRCan). The hyperspectral data were then compared to field sampled data to understand the biochemical distribution of nitrogen, total chlorophyll and moisture in the GVWD.

1.1 Research Objectives

The intention of this thesis is develop and validate methods of estimating biochemistry in forested environments using hyperspectral remote sensing data. In this research, methods of estimating canopy biochemical constituents are examined to determine the distribution of biochemicals in the GVWD. The research question addressed in this study is: Can airborne hyperspectral data be used to observe conifer biochemistry in the Greater Victoria Watershed District? If so, can the distribution of the biochemicals be mapped regionally?

The following objectives have been established in response to the research question:

- Establish a method of differentiating between Douglas-fir forest canopy and the influence of other forest species spectral signatures using unmixing techniques;
- Understand the relationship between the hyperspectral data and field sampled biochemistry data in the GVWD required for biochemical analysis estimation;
- Determine an appropriate statistical technique to estimate canopy biochemical constituents from site-specific biochemistry data and apply it to the entire hyperspectral data set;
- Map the biochemical distribution of the forested regions in the GVWD.

1.2 Organization of the Thesis

This thesis is organized into seven chapters. The rationale, study objectives and organization of the thesis are presented in Chapter 1. The principles of hyperspectral remote sensing are presented in Chapter 2. In Chapter 3, a literature review of hyperspectral remote sensing of forested environments is provided. The study site and data collected for this research are described in Chapter 4. Hyperspectral image processing, spectral unmixing and statistical techniques used to estimate forest canopy biochemistry are discussed in Chapter 5. In Chapter 6, results from the spectral unmixing and statistical analysis of the data are provided. Lastly, study conclusions and contributions of the research are contained in Chapter 7.

2.0 IMAGING SPECTROMETRY

With the launch of Landsat-1 in 1972, the ability to observe forests, over a large area on the earth, using optical remote sensing technology offered a non-destructive method of examining forest canopy attributes. Since that time, improved optical sensor technologies have been developed to image the Earth's surface, such as Système Pour l'Observation de la Terre (SPOT) and the National Oceanographic and Atmospheric Administration (NOAA) Advanced Very High Resolution Radiometer (AVHRR). While these broadband optical sensors had the capability to provide reflectance over a large area, the ability to resolve detailed spectral information of the features under examination was not possible due to the large bandwidths of the wavelength channels used for imaging (Green *et al.*, 1988).

With the engineering of high spectral optical sensors, a detailed investigation of the Earth's surface became possible. Imaging spectrometry, defined as the simultaneous acquisition of contiguous spectra, added another dimension to remote sensing (Lillesand and Kiefer, 1994). Hyperspectral remote sensing, synonymous with imaging spectrometry, provides the ability to identify features through absorption and reflectance characteristics (Curran, 1989). Hyperspectral sensors such as Airborne Visible/Infrared Imaging Spectrometer (AVIRIS), compact airborne spectral imager (*casi*) and space-based Hyperion and Compact High Resolution Imaging Spectrometer (CHRIS) are used in many applications of remote sensing such as geology (Kruse *et al*, 1993), soil studies (Palacios-Orueta and Ustin, 1996), coral reefs (Holden and LeDrew, 2001) and vegetation (Peterson *et al.*, 1988). These sensors, with various spectral, spatial and

temporal resolutions, provide a method of examining forested environments through classifying forests and assessing the biochemistry of these forests.

2.1 Applications of Imaging Spectrometry in Vegetation Studies

Remote sensing technologies provide a practical and feasible method of monitoring vegetation from a local to a global scale on a regular basis (Curran, 1989). Historically, *in situ* biochemical analyses were destructive to the vegetation, financially unfeasible and time consuming for investigators (Martin *et al.*, 1998). Throughout the history of remote sensing, vegetation analysis and classification have been the primary uses of spectral information derived from active or passive sensors on both satellite and aerial platforms. Imaging spectrometry applications in vegetation studies have intensified in the last 15 years with applications such as vegetation biochemistry and forest classification (Yoder and Crosby, 1995; Curran *et al.*, 2001). These issues are discussed in the remainder of the chapter.

2.1.1 Vegetation Biochemistry

Initially established in a laboratory, imaging spectrometry techniques progressed to allow for spectrometers on board airborne platforms to estimate foliar biochemistry (Peterson *et al.*, 1988). Hyperspectral sensors provide a detailed spectral signature of the forest canopy that can be used to estimate biochemical composition and map biochemical distributions in the forests (Wessman, 1990; Martin and Aber, 1997; Smith *et al.*, 2002).

Vegetation foliage interacts directly with incoming solar radiation; therefore, through examining the optical properties dependent upon the physiological state of the vegetation,

the biochemical characteristics of the foliage can be understood (Wessman, 1990). Assessing the biochemical constituents of the forest canopy allows for insight into ecosystem processes such as photosynthesis, evapotransporation and nutrient cycling (Curran, 1989; Aber and Martin, 1995; Kokaly and Clark, 1999). Peterson *et al.* (1988) note that the detection and measurement of forest canopy biochemistry can be used to predict biogeochemical processes such as plant productivity and litter decomposition. It is the identification of absorption and reflectance characteristics of the forest stands that allows the biochemical characteristics to be detected by hyperspectral sensors such as AVIRIS (Green *et al.*, 1988).

Biochemicals found in the forest canopy, including moisture, chlorophyll and nitrogen, possess absorption features in the visible to mid-infrared (400 nm to 2500 nm) portion of the electromagnetic spectrum (Peterson *et al.*, 1988; Wessman, 1990). It is the biochemical absorptions that are studied when measuring forest biochemistry. The amount of individual biochemical absorption is reliant on the plant tissue and is controlled by factors such as nutrient levels, light exposure and water deficiencies (Chapin, 1980). Knipling (1970) notes that all types of vegetation have sensitivities to biochemicals in the visible, mid infrared and near infrared regions of the spectrum. When properly calibrated, a spectrum is the combination of all absorption features of each chemical present in the vegetation, dependent on the concentration (Curran, 1989). Fluctuations in the absorption of canopy biochemicals can be used to determine overall plant health. Plant senescence as a result of disease, insect infestation, metal

contamination or water deficiency can be noted in the spectrum when imaged by a hyperspectral sensor (Ahern, 1988; Banninger, 1989; Gausman and Quisenberry, 1990).

Forest canopy biochemistry extracted from hyperspectral remote sensing data can be used as input into forest ecosystem models. Martin and Aber (1997) note the value of combining forest biochemistry with ecosystem models as an approach to assessing ecosystem processes. For example, nitrogen concentration was measured and used as input for carbon balance models. Later, in Smith and Martin (2001), the researchers note the importance of accurate estimation of biochemistry for forest modeling of growth and nutrient cycling.

While research into understanding the biochemical processes occurring in forested environments has improved over the last twenty years, the need to continue researching methods and refining technology is important to improve current methods of estimating biochemistry from remotely sensed data (Curran 1989; Yoder and Crosby, 1995; Ollinger *et al.*, 2002). Further refining methods of leaf and canopy level modeling, incorporating canopy structure and mitigating the contribution of background noise are required to improve biochemical contributions of ecosystem modeling (Serrano *et al.*, 2002).

2.1.2 Forest Classification

Image classification has typically been performed using optical multispectral remote sensing data; however, with detailed spectral information from hyperspectral sensors, forest cover information can be attained. Martin and Aber (1996) used AVIRIS data to produce species composition maps in forested environments. The AVIRIS data were used

along with GIS data derived from the field to determine the species distribution of 10 stands comprised of both mixed deciduous and conifer species. In a later study, Martin *et al.* (1998) were able to determine 11 forest classes of both deciduous and conifer species using AVIRIS data. Using a supervised classification the species in both pure and mixed stands were classified with the assistance of GIS forest cover data. In 2003, Kokaly *et al.* used AVIRIS data to classify land cover in Yellowstone National Park, USA. In this study both forested and non-forested land cover distributions were mapped.

Advanced Solid-State Array Spectroradiometer (ASAS) data were used by Sandmeier and Deering (1999) to determine the composition of the forests in boreal regions of Canada. The ASAS data, coupled with Bidirectional Reflectance Difference Function (BRDF) measurements, were used to differentiate among six forest cover classes including black spruce, jack pine, tamarack, spruce/pine, treed muskeg, and clear muskeg. The method of classification used in this study improved upon existing procedures for producing and maintaining forest cover maps.

Schmidt and Skidmore (2003) used field-based spectral measurements to differentiate among 27 salt marsh vegetation species in Holland. Spectral libraries derived from the field data were used to both calibrate and validate classification results. Radiometric calibration of the spectrometer data proved to be essential in determining vegetation species when using spectral libraries. Gong *et al.* (1997) also used field based spectral measurements to identify 6 conifer species in the central Sierra Nevada, USA. To

improve classification results ideal conditions, such as stable illumination, were required during hyperspectral data acquisition.

2.1.3 Red Edge Index

Typically red edge indices have been used in agricultural applications with narrow optical sensors; however, with the development of airborne and spaceborne hyperspectral sensors, red edge detection techniques can be used in forestry research. The red edge is the term applied to the inflection of the spectrum at approximately 740-760 nm as a result of the leaf chlorophyll content (Matson *et al.*, 1994; Clevers and Jongschaap, 2001). The high spectral resolution of hyperspectral data allows for the detection of this shift evident in narrow bands of the spectrum. The position of the red edge in the spectrum can shift as a result of decreased chlorophyll, in which case the inflection point is found in longer wavelengths.

Red edge indices have been examined using Radiative Transfer Models, such as SAIL, a canopy reflectance model, and PROSPECT, a leaf reflectance model. Daughtry *et al.* (2000) used field spectrometer data to examine leaf chlorophyll and nitrogen content. The position of the red edge was investigated along with LAI and Leaf Area Distribution (LAD) using the SAIL model to determine the biochemical properties of corn leaves.

2.2 Methods of Imaging Spectrometry in Vegetation Biochemistry Applications

When imaging spectrometry is used in vegetation applications, different methods of analysis are performed; these can include continuum removal, spectral unmixing and statistical modeling.

2.2.1 Continuum Removal

Continuum removal is a technique used to examine the absorption features of specific wavelength-sensitive components of a hyperspectral scene. Developed by Clark and Roush (1984), this method normalizes spectra resulting in a removal of unwanted noise to make the signal of interest detectable (Figure 1).

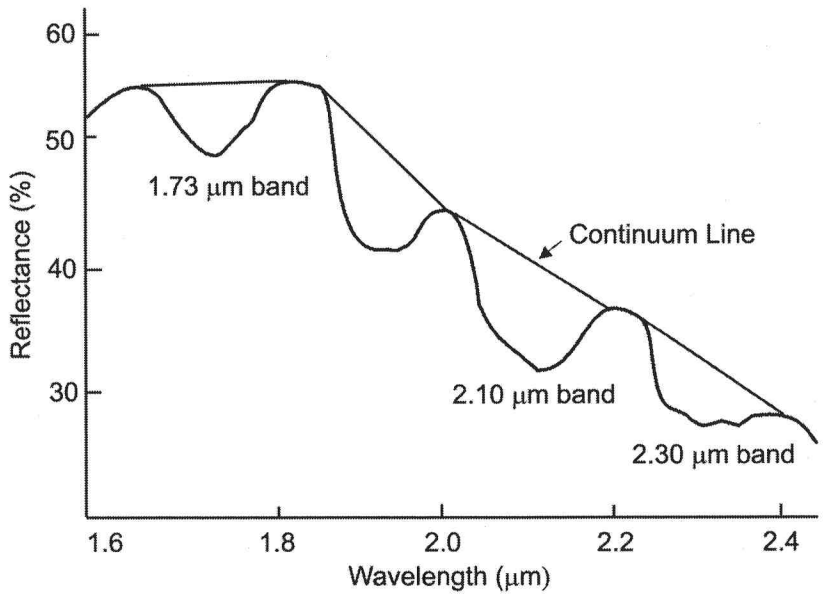

Figure 1: Continuum removed spectra
Adapted from: Kokaly, 2000, p. 154.

A continuum-removed spectrum is computed by dividing the reflectance value of each point in the absorption band by the reflectance of the continuum line at the corresponding band:

$$BNC = (1 - (R/R_i))/(1 - (R_c/R_{ic}))$$

"Where BNC is the band depth normalized to the centre, R is the reflectance of the sample at waveband of interest, R_i is the reflectance of the continuum line at waveband of

interest, R_c is the reflectance of sample at absorption feature centre and R_{ic} is the reflectance of continuum line at absorption feature centre (Curran *et al.*, 2001, p.350)".

The continuum removed features can then be compared using scaling factors and by comparing absorption shapes. Kokaly and Clark (1999) used the continuum removal method to estimate nitrogen, lignin and cellulose in mixed forest stands. It was found that the effects of sensor noise, atmospheric influences, leaf water content and unwanted background signal were reduced as a result of the continuum removal. In a later study by Kokaly (2000), the concentration of nitrogen in plant foliage was examined using continuum removal to provide an in-depth examination of the absorption features associated with nitrogen. In 2003, Kokaly *et al.* used continuum removal to examine the distribution of vegetation throughout Yellowstone National Park to produce vegetation cover maps with AVIRIS data.

Curran *et al.* (2001) examined the biochemical concentrations of pine canopies using field-based spectrometer data. A total of 12 biochemicals were examined, including chlorophyll *a*, chlorophyll *b*, total chlorophyll, lignin, nitrogen, cellulose, water, phosphorus, protein, amino acids, sugar and starch. Known absorption bands in the spectrometer data were analyzed using continuum removal to determine an estimate of concentration. When differentiating between salt march species, Schmidt and Skidmore (2003) used continuum removal to examine both the visible and near-infrared sensitivities of the biochemical absorptions.

2.2.2 Spectral Unmixing

Inherent in remote sensing data are mixed pixels, a combination of land cover types within one image pixel that blend together to become a spectrum (Verbyla, 1995) (Figure 2). This area of research has been addressed in geological applications (Mustard, 1993; Kruse *et al.*, 1997; Chabrillat *et al.*, 2000; Cudahy *et al.*, 2001) where many types of minerals are found on the ground contained within the spatial resolution of one image pixel. Recently, the use of spectral unmixing in vegetation applications has become of interest; however, due to the complexity of the spectral response of vegetation, it is difficult to accomplish using established methods where the same physical parameters do not exist (Small, 2001; Caetano *et al.*, 1997).

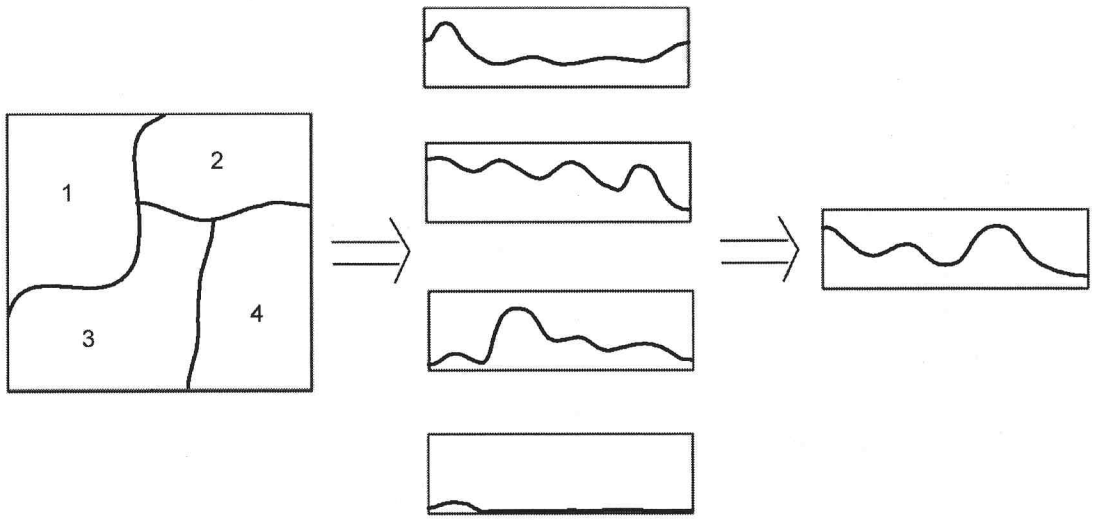

Figure 2: Spectral unmixing – pixel unmixing of spectra

Image classification using traditional techniques such as supervised and unsupervised classification, also known as hard classifiers, will result in assigning mixed pixels to classes using a statistical method based on the pixel value (Jensen, 1996). This results in one class type for each pixel; however, this does not adequately describe most forested

environments. In these environments, the influence of leaves, understory and shadow can contribute to the spectral signature of a pixel (Hurcom *et al.*, 1996). Spectral unmixing accounts for each component in the pixel, provided that the spectra are a linear combination of the pixel. The following represents a spectral unmixing model:

$$R_i = \sum_{j=1}^{n} f_j \mathrm{Re}_{ij} + \varepsilon_i \text{ and } 0 \leq \sum_{j=1}^{n} f_j \leq 1$$

where the spectrum of a pixel is R_i, the fraction of the components is f_j, the endmember is j, the band is i, Reij is the spectra for each n pixel in the image and ε is the residual error (van der Meer, 1999, p.187).

The unmixing model determines the spectral signature of each endmember in a pixel to create a set of endmember fraction estimates for each pixel, which can indicate the spatial distribution fraction of each endmember. Selecting these spectrally pure components, or endmembers, can be accomplished through two methods by using either "known" spectral signatures from a spectral library derived from field or laboratory research or "derived" spectral signatures employing the purest pixels in the image (van der Meer, 1999). After the selection of spectrally pure pixels, classification of the image into land cover types can be attempted. Often unmixing validation is attempted with field reconnaissance or with the assistance of *a priori* knowledge of the materials present at the site (Cudahy *et al.*, 2001; Small, 2001).

2.2.3 Statistical Modeling

Forest biochemistry and hyperspectral data have been integrated through statistical modeling. The statistical model is discussed in the following section of the chapter. A widely used statistical measure to predict biochemical concentrations from reflectance spectra is a multivariate linear regression (MLR) (Banninger, 1989; Matson *et al.*, 1994; Gastellu-Etchgorry *et al.*, 1995; Martin and Aber, 1996; Martin *et al.*, 1998; Curran *et al.*, 2001). The basis of a multivariate linear regression is the following model:

$$Y = a + b_1 x_1 + b_2 x_2 + \ldots + b_k x_k + e$$

where Y is the measured biochemical reference value, a is a constant, x_k is the measured signature value centered at the wavelength i, b_i is the best-fit coefficients, e is the error term (Chatterjee *et al.*, 2000).

Two methods of MLR have been applied to forest biochemical analyses; these include stepwise regression and Partial Least Squares (PLS) regression. Peterson *et al.* (1988) used stepwise regression to determine optimal wavelengths for predicting nitrogen from laboratory spectra. Reflectance values were converted to absorbance and their first and second derivatives for model computation. The regression model was validated using a cross-validation technique in which one third of the samples were predicted from the model. The result of the regression model was compared to wavelengths of known absorption features to further test the model. Results indicated that absorbance and first derivatives provided similar results when predicting nitrogen; however, second derivatives did not predict as well.

Wessman *et al.* (1988) used absorbance and first and second derivatives of laboratory-based hyperspectral data to examine the chemical composition of a mixed deciduous and coniferous forest stand. An MLR was used to assist in selecting a wavelength associated with nitrogen and lignin. In a similar study conducted by Peterson *et al.* (1988), approximately 30% of samples were held back to determine the strength of the model. First derivatives were found to be useful in predicting nitrogen concentration in mixed deciduous and coniferous forests. Wavelengths that were selected by the model were similar to those of known wavelength absorptions.

Curran *et al.* (1992) used stepwise regression to determine the relationship between laboratory-based hyperspectral reflectance and foliar biochemicals. In order to examine this relationship, four assumptions must be accepted: linearity between the variables, the ability to extract biochemical information from hyperspectral data, the influence of tree phenology or canopy geometry, and the ability to measure biochemicals from these models. With these assumptions in mind, the relationships between reflectance and foliar chlorophyll, protein, starch, sugar, amaranthin and water were examined with varying degrees of success. While stepwise regression models were able to predict some biochemicals, the method of detecting these components in laboratory spectra differed from the method used to do so in field spectra and should not be processed in the same manner. When wavelengths selected for inclusion in the model were compared, those that are not in known absorption bands or within 10 nanometres away from known sensitive regions were included in the model. These could be due to correlations between the biochemicals, instrument noise or a product of the stepwise regression procedure.

Yoder and Crosby (1995) used the first derivative spectra of both reflectance and absorbance to examine nitrogen and chlorophyll in broadleaf laboratory spectra. The stepwise regression models were computed with both calibration and validation data. Through model validation it was determined that not all known sensitivity bands were selected; however, due to the sample size the model proved to be adequate. The first difference transformation of the spectra was found to be successful in removing some spectral noise; however, a shift in the wavelengths could influence their correlation. Given that this study was conducted in a laboratory, the authors discuss issues related to similar studies conducted in the field, such as the angle of the solar illumination, the geometry of the forest canopy and the sensor field of view.

Gao and Goetz (1995) used stepwise regression modeling to examine canopy lignin in a mixed deciduous conifer forest. While the model was computed using site-specific spectral data; the issue of applying this model to other sites, without ground calibration, was addressed. It was determined that further testing was required to validate the application of site-specific regression models. A similar study by Johnson and Billow (1996) used stepwise regression to model nitrogen in laboratory spectra of Douglas-fir foliage. The spectra were converted to first derivatives to emphasize subtle changes in the slope at each wavelength possibly associated with nitrogen absorption. A cross validation technique was used to validate the regression model indicating the ability to detect nitrogen features and noise in the spectral data.

Martin and Aber (1997) use stepwise regression to examine AVIRIS data and field measured foliar nitrogen and lignin. The hyperspectral data were converted to first derivatives for use in the modeling. To further improve upon model results, an input of detailed species map would have been useful. The authors note the contribution of forest biochemistry models to understanding carbon balance and nitrogen cycling in the forest canopy and as inputs to ecosystem modeling.

Serrano *et al.* (2002) used stepwise regression along with first derivatives of AVIRIS reflectance to determine canopy biochemical concentrations in chaparral vegetation. The model was validated using correlation values and standard error techniques. Through the modeling it was noted that the stepwise regression model did not provide consistent results when applied to different vegetation types.

Another method of multiple linear regression used to examine canopy biochemical concentrations is Partial Least Squares (PLS). This method, described in detail in chapter five, is a three-step regression that uses both the independent and dependent variables to compute a new set of variables (latent) that are used in the modeling (Garson, 2002). All of the wavelengths in the hyperspectral dataset are used; however, loadings are computed to determine the contribution of each wavelength to the latent variables. Input into the PLS model can include reflectance, absorbance and their derivatives. The remote sensing community has explored this method of regression in vegetation studies in the last few years.

Ollinger *et al.* (2002) used PLS to examine canopy biochemistry in 30 broadleaf forest stands. Absorbance values of AVIRIS data were computed to provide input into a model

for foliar nitrogen concentrations. Through the PLS regression, the hyperspectral data were reduced to a smaller set of independent variables that were used for the nitrogen concentration prediction. The resulting model, computed from the chemistry sample plots, consisted of a 2-factor equation with a correlation coefficient of 0.69 for nitrogen. This model was then applied to all of the AVIRIS scenes to provide a map of nitrogen distribution in the entire forested area. This method of regression modeling is said to be the most accurate for representing variations in the canopy biochemistry of forest canopy as it provides more accurate estimates of canopy biochemistry and includes both the independent and dependent variables in the model computation (Ollinger *et al.*, 2002).

Smith *et al.* (2002) used PLS to identify the best prediction model for estimating foliar nitrogen in mixed deciduous and coniferous forest stands. Absorbance and first derivatives of AVIRIS data were used to compute a 3-factor model for predicting nitrogen. The efficiency of the model was validated using coefficient of determination, residual plots and regression probability values. After validation the model was then applied to the entire forested area evident in the AVIRIS data.

2.3 Chapter Summary

The importance of imaging spectrometry and forestry applications has been discussed in this chapter. The applications of hyperspectral remote sensing in forestry, including biochemistry, classification and red edge detection, have been discussed. The methods in which forest biochemistry has been examined, including spectral unmixing, continuum removal and statistical modeling, have been discussed. The following chapter provides a

basis of understanding of the interaction of incoming solar radiation and the forest canopy to further illuminate the canopy biochemistry.

3.0 HYPERSPECTRAL REMOTE SENSING OF VEGETATION

In order to interpret the response of vegetation in the GVWD, as captured by a hyperspectral sensor, it is necessary to understand of plant and incoming solar radiation interactions; that is, how incoming energy photosynthetically reacts to leaf (interchangeable with needle) and canopy structure and composition to provide a spectral response of the vegetation. This spectral response is then analyzed for vegetation biochemical components.

3.1 Spectral Response of Vegetation

The spectral response of vegetation is reliant on both leaf and canopy characteristics. As a healthy green leaf intercepts energy directly from the sun or from diffuse sunlight, energy interacts with pigments, water and intercellular air spaces at the foliar level (Gausmann and Quinsenberry, 1990). The interaction of this incoming energy influences the reflectance, scatter and absorbance properties of the leaf. The reflectance of foliage can be described as equal to the incident energy minus the energy absorbed directly by the plant and the amount of energy transmitted directly through the leaf (Jensen, 2000). The interaction of energy at the leaf level contributes to the overall reflectance of the forest canopy.

At the foliar level, incident energy reacts with the upper epidermis transferring the energy into the leaf (Figure 3). The cuticle then diffuses the energy throughout the leaf, reflecting little to no energy. The light energy is then scattered, both Rayleight and Mie scattering, to the palisade parenchyma cells, which house chloroplasts containing chlorophyll *a* and *b* pigments.

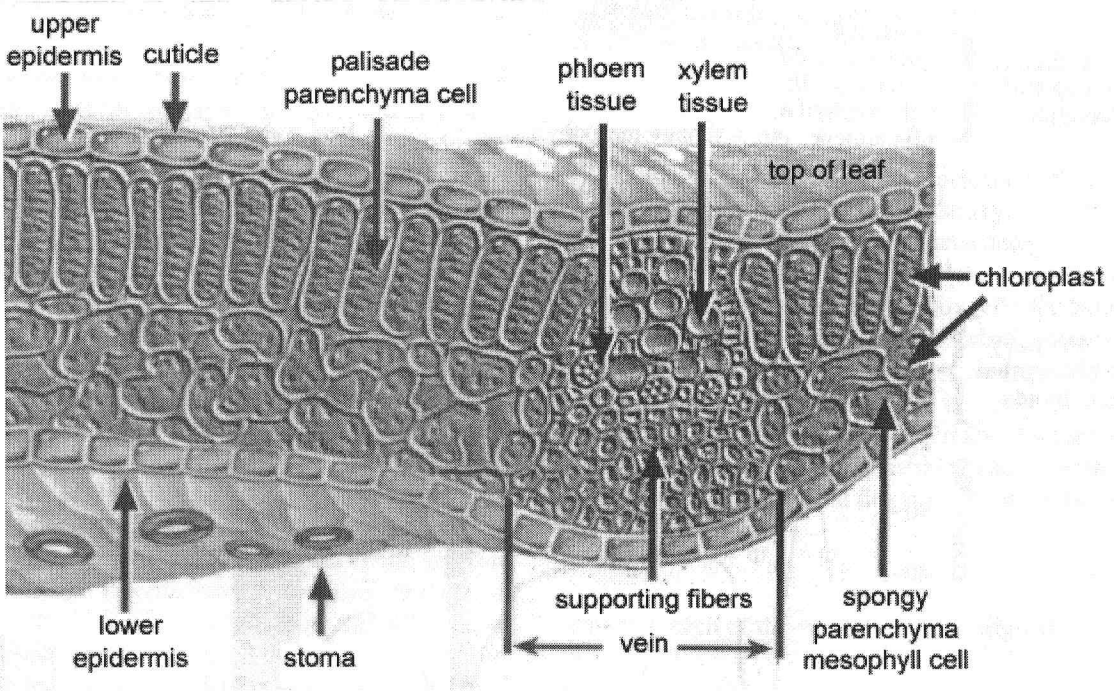

Figure 3: Cross-section of a healthy plant
Source: Jensen, 2000, p. 336.

The abundance of chloroplasts in the upper portion of the leaf interact with visible energy and absorb blue and red light required for photosynthesis, which is why healthy vegetation appears green in colour. The palisade cells also contain carotenes and xanthophylls that absorb energy in the blue region of the spectrum. The lower portion of the leaf contains spongy parenchyma mesophyll cells that interact with infrared energy to diffuse reflectance according to the characteristics of the plant cell walls. Within the spongy parenchyma mesophyll cells, very little infrared energy is absorbed, approximately 5-10 percent. However, high amounts of incident infrared energy are transmitted, approximately 40-60 percent, and the remaining 40-60 percent is then reflected from these cells (Jensen, 2000). Incoming energy that is neither absorbed nor reflected penetrates through the leaf mesophyll and is transferred out through the stoma in the lower epidermis (Gausmann and Quinsenberry, 1990).

Reflectance, scatter and absorbance processes occurring within a leaf are evident in the visible to mid-infrared portions of the spectrum and can be used to provide information on vegetation health (Wessman *et al.*, 1988). The spectral response of healthy green vegetation is characterized by a decrease in reflectance in the blue region (400-500 nm), increased reflectance in the green region and a decrease of reflectance in the red region (Figure 4).

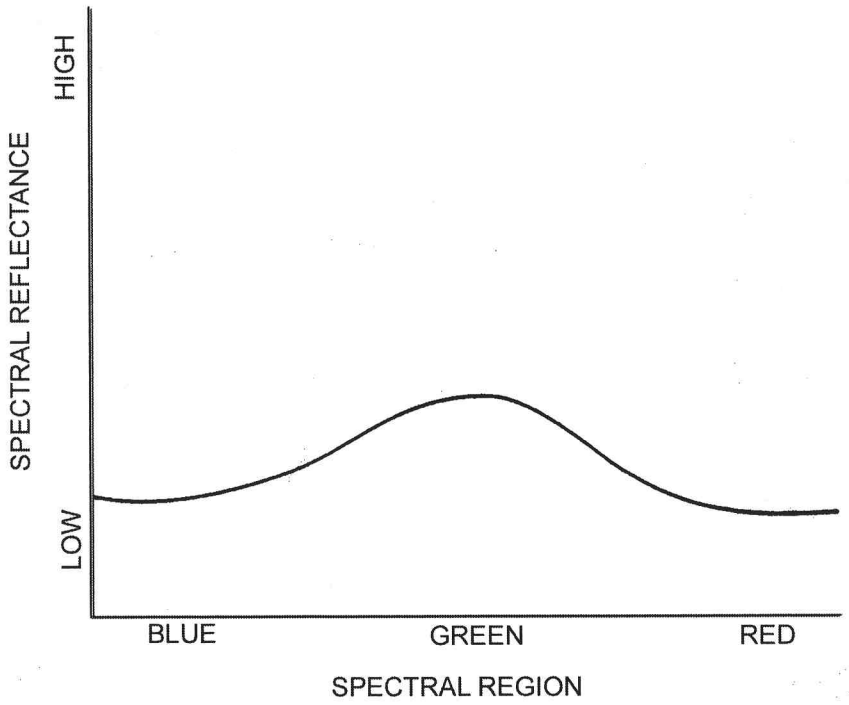

Figure 4: Response of vegetation in the visible portion of the spectrum
Source: Verbyla, 1995, p. 48.

An abrupt increase in reflectance in the near infrared wavelengths, at approximately 700-740 nm, is noted for healthy green vegetation. The near-infrared portion of the spectrum

is characterized by high reflectance values with decreasing reflectance in the mid-infrared portion for healthy green vegetation (Figure 5).

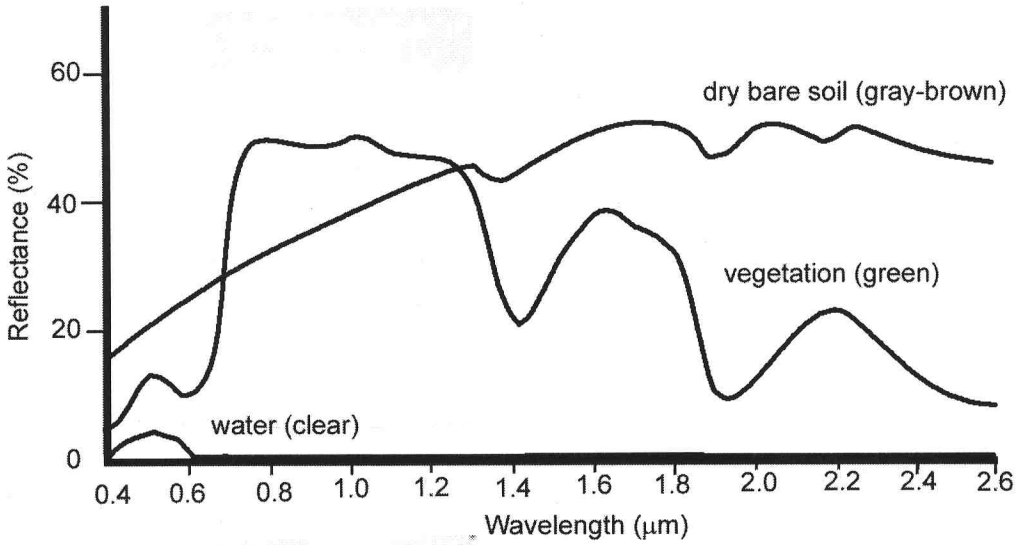

Figure 5: Typical spectral curves from vegetation, soil and water
Source: Lillesand and Kiefer, 1994, p. 18.

As a plant enters senescence, the final stage of plant life, chlorophyll content decreases faster than carotenes resulting in an increase of reflectance in red wavelengths due to an increase of absorption in blue wavelengths. Reflectance in the near infrared decreases as a result of collapsed mesophyll cells in the plant tissue during senescence (Broge and Leblanc, 2000). As foliage expires, tannins contained within the leaf cause the reflectance to decrease and the leaf to appear brown (Kumar *et al.*, 2001). A detailed description of the energy characteristics in the visible, near and mid-infrared portions of the spectrum is provided below.

3.1.1 Visible Light Interaction

The visible portion of the spectrum, 400-700nm, is characterized by low reflectance and transmittance due to the absorption of energy by leaf pigments. Incident energy absorbed in this portion of the spectrum is used for plant photosynthesis and photochemical reactions, with the exception of energy in the green portion. The absorption of chlorophyll *a* and *b* in this portion is critical for plant photosynthesis, and thus plant growth. Figure 6 illustrates the absorption characteristics of chlorophyll in the visible portion of the spectrum.

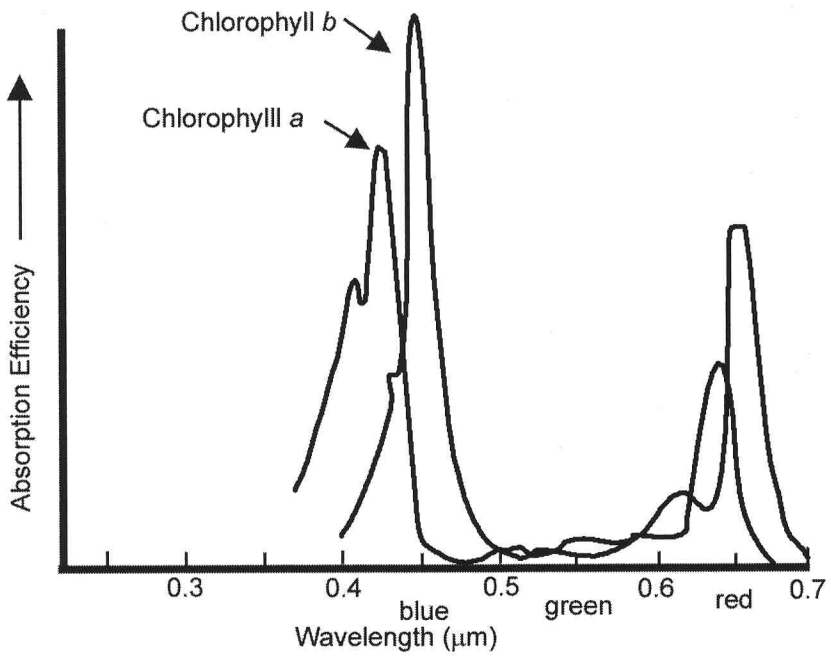

Figure 6: Absorption spectra of chlorophyll a and b pigments
Adapted from: Jensen, 2000, p. 338.

3.1.2 Near-Infrared Light Interaction

The reflectance of healthy green vegetation in the near infrared portion of the spectrum, 700 to 1300 nm, is characterized by a marked increase in reflectance at approximately 690 to 720 nm, known as the red edge, with continued high reflectance through to the mid-infrared region. Internal leaf structure and water content dominate reflectance in this region where very little energy is absorbed or used for photosynthesis, rather it is reflected or transmitted (Riggs and Running, 1991; Kumar *et al.*, 2001). Energy absorbed in the near and mid infrared portion of the spectrum is primarily used for evaporation and transpiration (Gausmann and Quisenberry, 1990). Forest canopies appear to be highly reflective not only due to the high amount of leaf reflectance, but also due to the high amount of energy transmitted to leaves below, which is then also potentially reflected, the process being known as leaf additive function (Verbyla, 1995).

The near infrared region is particularly useful for differentiating forest classes since the internal cellular structure of plants varies with each species exhibiting unique reflectance properties. Plant senescence or stress, specifically water stress, can also be examined using reflectance present in the near-infrared region, due to the sensitivity of this region to water content (Pierce *et al.*, 1990; Riggs and Running, 1991; Kumar *et al.*, 2001) (Figure 7).

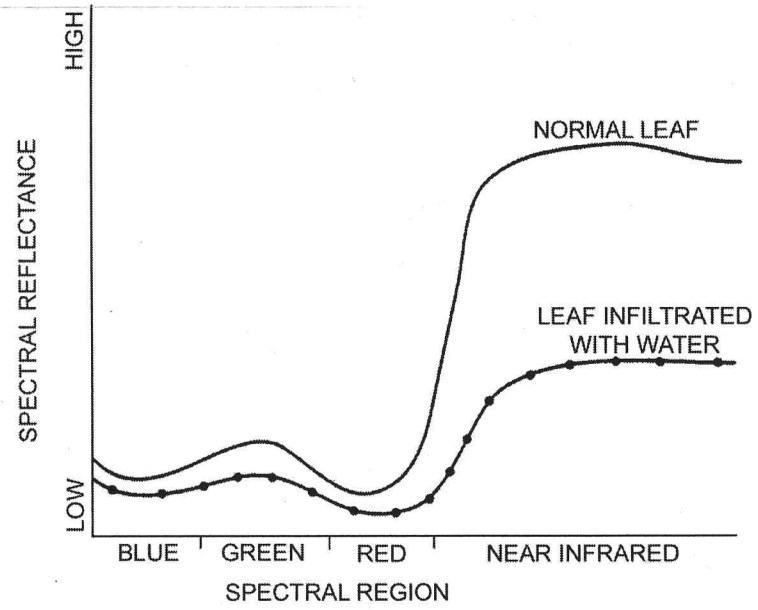

Figure 7: Spectra for a healthy and water stressed leaf
Source: Verbyla, 1995, p.50.

3.1.3 Mid-Infrared Light Interaction

The reflectance of vegetation in the mid-infrared portion of the spectrum, 1300 to 3000 nm, is a function of the total amount of leaf water content and leaf thickness. The sensitivity of the mid-infrared region to leaf water content is useful for detecting water stress, due to the capability of water to absorb mid-infrared energy; thus when leaves are turgid, reflectance values will be lower (Pierce *et al.*, 1990). As water content in a leaf decreases, the amount of intercellular space becomes greater in a leaf, so mid-infrared energy will scatter at the interface of the intercellular walls resulting in an increase in leaf reflectance (Jensen, 2000). The contribution of leaf and canopy characteristics to overall vegetation reflectance is discussed in the following sections.

3.2 Leaf Reflectance

Leaf reflectance contributes to and is evident in overall canopy reflectance. Hyperspectral remote sensing can be used to examine internal leaf optical properties, which are influenced by pigment composition, leaf structure, water content, age and nutrient content. The response of vegetation, as imaged by spectrometers, is the result of the interaction between incoming solar radiation and various structural components of individual leaves. These components have sensitivities in the visible to mid-infrared wavelengths that when coupled with canopy reflectance models can be used to illuminate the biochemical processes occurring within a forested environment.

3.2.1 Pigment Composition

The pigment composition of plant foliage contributes to the reflectance of an individual leaf. In healthy green vegetation, an abundance of chlorophyll pigments can be found in both the palisade parenchyma and spongy parenchyma mesophyll cells, thus allowing photosynthetic activity to occur (Moran *et al.,* 2000). Along with chlorophyll, pigments such as carotenes and xanthophylls, required for plant development, can be found in plant cells. The presence or absence of pigments contained in plant cells is evident in absorption bands in the visible region of the spectrum, which can be imaged by hyperspectral sensors. The abundance of foliar pigments is dependent on age and time of year, particularly in deciduous and mixed broadleaf forests (Jensen, 2000).

3.2.2 Leaf Structure

The internal and external characteristics of leaves differ both within tree species and between tree species. For example, in the Douglas-fir species, the leaf mesophyll is differentiated into two layers; the upper layer contains palisade parenchyma cells and the lower layer contains spongy mesophyll parenchyma cells, these providing different functions for photosynthesis (Kramer and Kozlowski, 1979). It is the internal structure of a leaf that determines the amount and interaction of energy as imaged by a spectrometer. The characteristics of the internal structure of a leaf depend primarily on its age; young and old trees exhibit different structural features such as amount of cells and stoma. The external properties of a leaf's structure can be influenced by canopy level, leaves in the upper canopy being rounder than those at lower levels in several tree species (Apple *et al.*, 2002).

3.2.3 Water Content

Water, necessary for plant growth and development, influences processes such as photosynthesis, evapotranspiration and respiration (Serrano *et al.*, 2002). The amount of water contained in spongy mesophyll cells is dependent on the stage of growth as well as species type (Riggs and Running, 1991). Leaf water content is evident in hyperspectral remote sensing data, specifically in the near and mid-infrared regions of the spectrum, where water in the spongy mesophyll cells interacts with incoming energy (Broge and Leblanc, 2000; Ceccato *et al.*, 2001). Conifer environments are ideal for studying water stress because during times of insufficient water, either due to lack of precipitation or soil moisture, the needles do not wilt or droop. The reflectance of the needles is then due

solely to insufficient water and not to fluctuations in canopy geometry (Riggs and Running, 1991).

Water absorbs energy in the near and mid-infrared regions; therefore leaves that are turgid will not reflect as much energy as leaves that are in conditions of water stress. The decrease of water within a plant causes cells to collapse, which results in air pockets inside the leaf mesophyll and an increase in the scattering of light. Gausmann and Quinsenberry (1990) discuss the increase in reflectance of diseased leaves in the near infrared region due to a decrease in leaf water content.

3.2.4 Age

The age of a leaf dictates the internal structure and thus influences its overall reflectance. The internal structure of a young leaf is compact with fewer air spaces in the mesophyll, whereas older leaves are typically less organized and contain fewer cells. In Douglas-fir species, trees with older needles can have 11% fewer mesophyll cells than younger needles, which affect photosynthetic ability and carbon accumulation (Apple *et al.* 2002). As a leaf ages, the ability to photosynthesize decreases, which in turn slows the overall tree growth rate.

3.2.5 Nutrient Content

The nutrient content of a leaf impacts the overall reflectance of a plant, specifically in the near and mid-infrared regions. Nutrient stress, defined as a disturbance that adversely affects the growth and development of a plant (Curran *et al.*, 2001), can be the result of water deprivation, internal cellular changes, insect infestation or disease. Leaves of

stressed plants show a lower reflectance in the visible and higher in the near and mid-infrared regions of the spectrum than healthy vegetation (Ceccato *et al.*, 2001). The reflectance of plants is influenced not only leaf properties but also by canopy characteristics.

3.3 Canopy Reflectance

While canopy reflectance is a function of individual leaf reflectance, overall canopy reflectance is also influenced by variations in ground cover, leaf area index (LAI), leaf angle distribution (LAD), bi-directional reflectance distribution function (BRDF) and time of year. A significant modification of any of these variables is required to influence the reflectance of the forest canopy (Gong *et al.*, 1997). For this reason, a priority at the time of image acquisition is to acknowledge these parameters in order to extract biophysical attributes of the forest canopy.

3.3.1 Ground Cover

The type of ground cover imaged by a spectrometer influences forest canopy reflectance. Since species differ in physiology, each exhibits unique spectral responses in the visible to mid-infrared regions that can be imaged by hyperspectral sensors. The ability to differentiate between forest species reflectance is a major research problem in hyperspectral remote sensing (Figure 8).

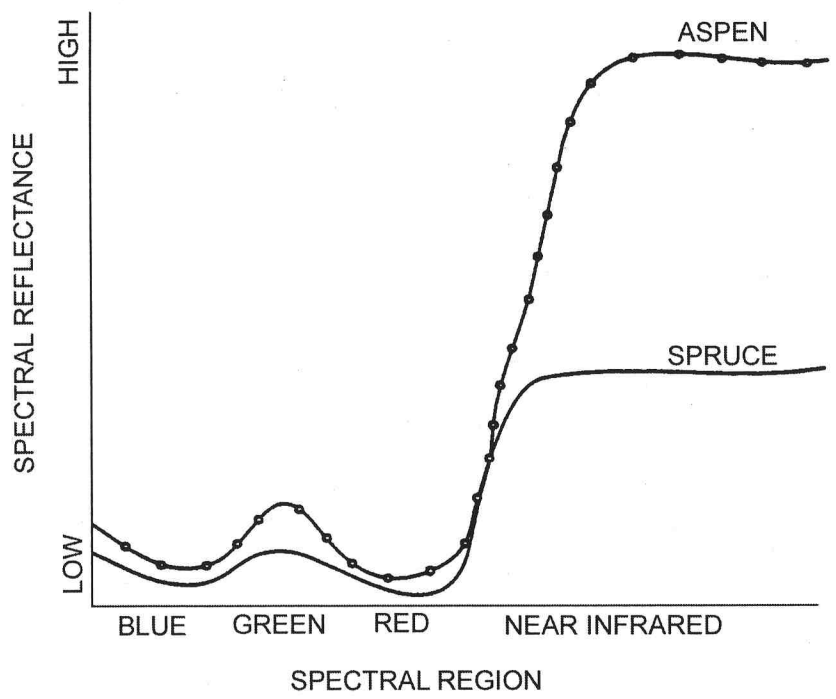

Figure 8: Reflectance of a broadleaf and a conifer tree species
Source: Verbyla, 1995, pg.52.

3.3.2 Leaf Area Index (LAI)

The quantity of ground cover influences the reflectance of a forest canopy. Leaf Area Index (LAI) is defined as the total green leaf area per unit of ground surface area (Wulder *et al.*, 1998), and it is thus the forest cover area that interacts with solar radiation. Although LAI varies spatially and temporally in forested environments, this parameter determines the exchange of carbon, water, nutrients and light at the ecosystem level. Thomas and Winner (2000) note annual fluctuations in LAI can occur as a result of climate variability, phenology and successional change in species composition. Douglas-fir foliage is heavily concentrated in the most exposed portions of the crown; these stands typically exhibit high measures of LAI (Thomas and Winner, 2000). In dense vegetation,

the reflection of red energy decreases while reflectance in the near infrared increases due to greater chlorophyll absorption. Canopies that do not have 100 percent closure allow features underneath to be included in the hyperspectral image creating a mixed pixel.

3.3.3 Leaf Angle Distribution (LAD)

Leaf Angle Distribution (LAD) influences the spectral response of forest canopies. The distribution of leaves is a phenological function, which determines whether leaves lie horizontally or vertically (Jensen, 2000). The distribution of leaves fluctuates on a temporal basis, both daily and seasonally. During the day, leaves may move toward the sunlight during photosynthesis. Since reflectance in the near infrared region is particularly dependent on the shape and orientation of the plant leaves, understanding the LAD characteristics of vegetation understory is important for comprehending the spectral response of vegetation (Verbyla, 1995).

3.3.4 Bi-directional Distribution Function (BRDF)

Vegetation is not considered to be a true Lambertian surface; therefore the amount of energy reflected from the surface is not uniform in all directions. BRDF is the ratio of the radiance reflected in one direction to the sun's incident irradiance (Jensen, 2000). The BRDF of vegetation is reliant on forest cover type and density, canopy illumination and sensor geometry. BRDF has an inverse relationship with reflectance; when reflectance is low, BRDF is more pronounced and vice versa (Sandmeier *et al.*, 1999). In particular, BRDF influences reflectance in the blue and red chlorophyll absorption bands, 480nm and 675 nm respectively, and in the low absorbing near infrared region.

3.3.5 Temporal

The time of day (morning, afternoon and evening) and time of year (spring, summer, fall and winter) of image acquisition influences canopy reflectance. The time of day determines the leaf water content, as fluctuations occur on a diurnal basis with the highest amount of water at pre-dawn as a result of water uptake from the soil. The lowest amount of water can be found in the afternoon when the transpiration rate exceeds the water uptake rate (Pierce *et al.*, 1990). The time of year influences plant phenology, which in turn influences plant reflectance. During productive growth periods, such as bud flush, changes in reflectance can occur. During the fall, chlorophyll pigments begin to diminish causing the needle to be dominated by pigments such as carotenes and xanthophylls (Verbyla, 1995). Climate can also influence the temporal nature of phenology, where high levels of precipitation or extended periods of drought throughout the year can affect plant growth and development.

3.4 Chapter Summary

In order to interpret the response of vegetation in the GVWD, as captured by the hyperspectral sensor, an understanding of plant interaction with incoming solar radiation is required. Internal and external leaf structural characteristics influence reflectance responses in the visible to mid-infrared regions of the spectrum. It is important to understand both the leaf and canopy characteristics influencing the reflectance of forested environments in order to estimate the overall health of vegetation. The study site and data collected for this research are discussed in the following chapter.

4.0 STUDY AREA AND DATA COLLECTION

This chapter describes the study location and the data collected for this research. The forest composition, history, topography and climate of the Greater Victoria Watershed District (GVWD) will be presented. Foliar chemical, hyperspectral airborne, field spectrometer and Geographic Information System data collected from the GVWD will be given.

4.1 Study Area

Located on Vancouver Island, British Columbia, the GVWD is situated at approximately 48.50° North latitude and 123.00° West longitude. Encompassing the Sooke and Goldstream watersheds, the GVWD is the source for the City of Victoria's water supply (Figure 9).

The 3132 hectares of land in the watershed contain lakes, forests and a variety of animal species. Forested land in the GVWD consists predominantly of Coast Douglas-fir (*Pseudotsuga menziesii*), with secondary species including Western Hemlock (*Tsuga heterophylla*), Western White Pine (*Pinus monticola*), Lodgepole Pine (*Pinus contorta*), Red Alder (*Alnus rubra*), Western Redcedar (*Thuja plicata*) and Arbutus (*Arbutus menziesii*). Ground cover includes a mixture of Salal (*Gaultheria shallon*), Bracken Fern (*Pteridium aquilinum*), Feathermoss (*Kindbergia oregana*), Oregon Grape (*Mahonia nervosa*), White-Veined Wintergreen (*Pyrola picta*), Salmonberry (*Rubus spectabilis*) and Tufted Hairgrass (*Deschapsia cespitosa* ssp. *beringenis*) (Brix, 1992).

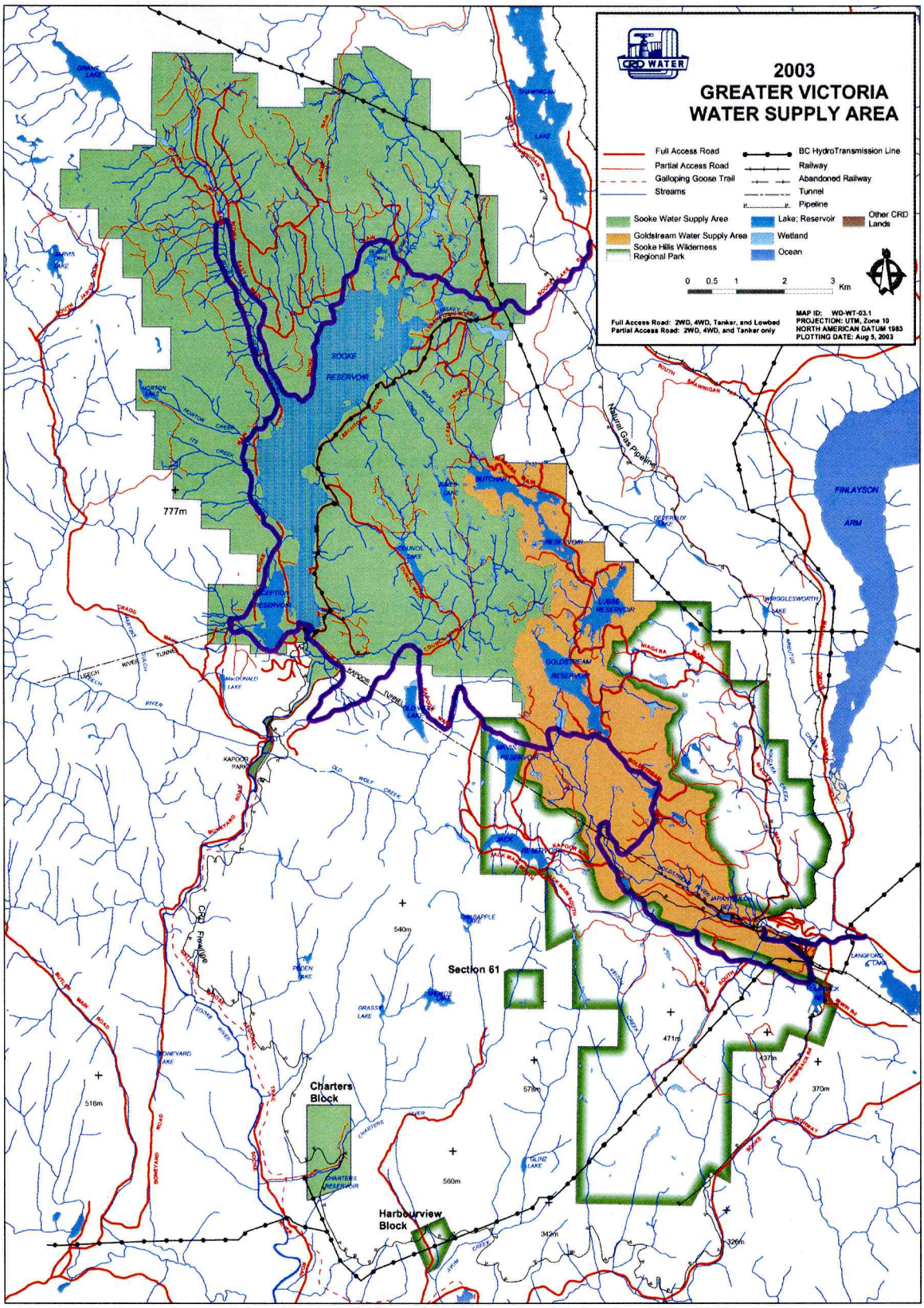

Figure 9: Location of the Greater Victoria Watershed District (GVWD)
Source: Capital Regional District, 2003.

Although many areas of the watershed have been logged and reforested in the last 100 years, the GVWD contains some of the oldest stands of Douglas-fir in the southern half of Vancouver Island (Goodenough *et al*, 2001). Past logging activity has resulted in various age classes in the second growth forest stands. Not only have logging activities influenced the growth of Douglas-fir in the GVWD but, in 1925, a number of stands in the watershed were burned by a wildfire. The burned forests were then regenerated, only to be destroyed by another fire in 1942. The second fire left the burned area with a thin humus layer, thus replanting of Douglas-fir did not occur until the spring of 1948 (Brix, 1992). With the exception of younger Douglas-fir stands, the old growth forest in the GVWD is largely unmanaged (Niemann, 1995).

The GVWD is topographically diverse with a relief of approximately 600 metres and an average elevation of 400 m above sea level. The terrain in the GVWD is diverse with slopes attaining gradients as great as 45 degrees (Goodenough *et al*, 2001). Soils in the GVWD are classified as Orthic Dystric Brunisol, which means they are characterized by loam and silt glacial till underlain by impermeable basal till. The well-drained layer of glacial till is shallow due to prior burning, resulting in a low percentage of carbon (C) and nitrogen (N) (Brix, 1992).

With 180 frost-free growing days (Hall, 1957), the GVWD is located in the Coastal Western Hemlock, Coastal Douglas-Fir and Mountain Hemlock biogeoclimatic zones (British Columbia Ministry of Forests, 1991). These zones are characterized by a high mean annual precipitation with episodes of drought in July and August and excess

precipitation in the winter months. The GVWD has a mean annual precipitation of 1217 mm, varying from 27 mm in the driest month to 207 mm in the wettest. During the last 4 months of the year, an annual water deficit of 192 mm occurs (Goodenough *et al.*, 2001).

4.2 Data Collected

In order to examine the biochemical characteristics of the forests in the GVWD, foliar chemistry, hyperspectral remote sensing, field spectrometer and GIS data were acquired. Data were collected as part of the Evaluation and Validation of Earth Observation for Sustainable Development (EVEOSD) project at the Pacific Forestry Centre.

4.2.1 Foliar Chemistry Data

The Pacific Forest Centre (PFC) collected samples of foliar chemistry from the GVWD in the summer of 2000 and 2001. Fifty-four ground calibration sites were selected throughout the GVWD representing a range of forest characteristics (Figure 10).

Plots containing old growth, mature and immature Douglas-fir stands in a range of various slopes, aspects and elevations were sampled. Within a 200 square kilometre area, a total of 1846 foliar samples of Douglas-fir and salal were collected during the field campaigns. Ancillary information gathered at the time of sampling included geographic position, site classification, dominant canopy, middle canopy and ground cover.

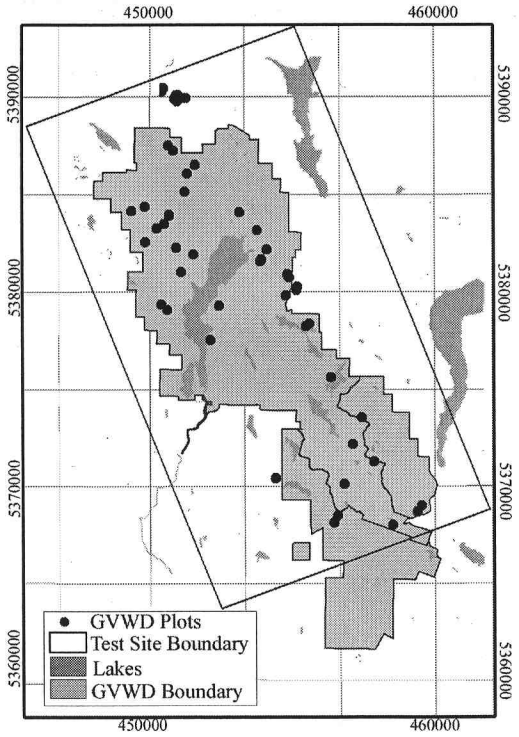

Figure 10: GVWD sample chemistry plots
Source: Goodenough *et al.*, 2003, p. 1322.

In September 2000, 10 trees in each of the 54 plots were sampled for foliar chemistry; these were then revisited in July 2001 when the first tree in each plot was re-sampled. Both current and non-current chemistry were sampled; due to the discrepancy in the time of year the samples were collected, the correlation between non-current sampled data proved to be appropriate for use with higher correlation than current chemistry. Douglas-fir foliage was collected from a helicopter along with a differential Global Positioning System (GPS) to provide positioning to accuracies within 1 metre. A ground crew collected salal foliar samples with a GPS to provide accurate geographic positioning. Five photographs facing north, south, east, west and the center were taken at each plot

and in summer 2000, 360° photographs from each site were acquired. The helicopter and ground foliar samples were then analyzed for biochemical constituents.

Foliar samples were divided into current and non-current growth to differentiate between growth that had occurred within the last year and that of previous years. The Pacific Forestry Centre then analyzed the samples for organic constituents, chlorophyll *a* and *b*, total chlorophyll, moisture percentage and nitrogen percentage. The chemical analysis was conducted using a field moisture measurement of wet weight and dry weight.

4.2.2 Airborne Visible/Infrared Imaging Spectrometer (AVIRIS) Data

Data from Airborne Visible/Infrared Imaging Spectrometer (AVIRIS) flown on the NASA ER-2 aircraft were acquired on August 10, 2001 over the GVWD coinciding with field spectra sampling. The AVIRIS sensor, designed by the Jet Propulsion Laboratory (JPL), has the capacity to capture 224 contiguous spectral bands at approximately 10 nanometre intervals. The four spectrometers (A, B, C and D) onboard AVIRIS image spectral ranges of 400-700 nm, 700-1300 nm, 1300-1900 nm and 1900-2500 nm of the electromagnetic spectrum (Green *et al.*, 1998). The whiskbroom scanner, scanning at a rate of 12 Hz, covers an 11 kilometre swath with a 20 metre spatial resolution (JPL, 2003). In total, six AVIRIS scenes (Figure 11) were required to image the entire watershed (Table 1).

Table 1: AVIRIS scenes from the GVWD UTM Zone 10 NAD 87

District	Scene	Easting	Northing	Pixels	Lines
1	1	454060.00	5385860.00	614	512
1	2	455480.00	5377240.00	614	512
1	3	457300.00	5370300.00	614	287
2	1	446720.00	5384700.00	614	512
2	2	448520.00	5375980.00	614	512
2	3	450160.00	5367640.00	614	454

Figure 11: Mosaic of six AVIRIS scenes

4.2.3 Ground Spectrometer Data

Ground radiance measurements were taken within the GVWD at established sites for airborne hyperspectral data calibration. An Analytical Spectral Devices (ASD) FieldSpec FR ground spectrometer was used by the EVEOSD team to collect 3,900 spectra over two calibration sites, a homogeneous field and Shawnigan Lake. Over a two-week period coinciding with AVIRIS overflights and foliar sampling, spectral measurements of Douglas-fir and salal stacks were taken in direct sunlight as well as shade. Other spectrally significant features of the watershed were also imaged, including various grass types, gravel and dirt roads and an asphalt parking lot. The geographic positions of each spectral signature collected were recorded by a GPS and photographed. The radiance spectra acquired for each target were converted to reflectance using a standard white reference both in the laboratory and in the field.

4.2.4 Geographic Information System Data

The Capital Regional District (CRD) provided digital Geographic Information System data about the watershed. The data included forest cover, hydrology and topography. The forest cover layer provided information including species type, age class and stand density. The GIS data were used in conjunction with 1 metre orthophotographs, taken on July 25, 1998, of the watershed in order to provide detailed information on the composition of each pixel in the hyperspectral data.

4.3 Chapter Summary

This chapter has described the GVWD and data collected for understanding the ecosystem processes in this area. In order to make clear the environmental characteristics of the watershed, the forest composition, history, topography and climate were surveyed. Knowledge acquired of the watershed included foliar chemical, hyperspectral airborne, field spectrometer and Geographic Information System data. Methods used to extract biochemical estimates and map the biochemistry in the GVWD are described in the following chapter.

5.0 METHODS

To assess forest canopy health in the GVWD, the AVIRIS data were preprocessed and processed to extract estimates of biochemical components. Preprocessing of these data included atmospheric and geometric correction to represent the atmospheric and topographic conditions at the time of image acquisition over the forest canopy. In order to compare the AVIRIS scenes over the watershed, the data must be properly calibrated to correspond with ground reflectance (Green *et al.*, 1991). To calibrate the AVIRIS data, a technique, based on ground spectrometer data, was applied to the AVIRIS imagery to further correct the airborne spectral measurements. Subsequent to image preprocessing, the resulting AVIRIS data are a closer approximation to a representation of the energy characteristics of the earth at the time of image acquisition. The hyperspectral data were then prepared for spectral unmixing and statistical analyses. The following chapter describes the atmospheric and geometric correction, spectral calibration, pixel unmixing and integration of hyperspectral and chemical data through statistical analyses.

5.1 Atmospheric Correction

When imaging vegetated land cover, it is important to mitigate the influence of the atmosphere on the energy incident on the Earth's surface (Griffin *et al.*, 1999). The atmosphere is composed of many kinds of particles which have absorptions in the visible and near infrared regions of the spectrum, oxygen, water vapour and ozone being among the most important (Broge and Leblanc, 2000). These absorptions can influence and alter the spectral response of vegetation. It is therefore important to identify, or approximate, the composition of the atmosphere during atmospheric correction (Gao *et al.*, 1991). This is particularly important when examining vegetation biochemical constituents, since

subtle differences in the reflectance of certain features are not easily separated from atmospheric constituents (Kokaly and Clark, 1999). The goal of atmospheric correction is to rectify distortion, degradation and noise inherent in the data caused by atmospheric composition (Jensen, 1996). During atmospheric correction, radiance values detected by the sensor are converted to reflectance (Clark *et al.*, 2002). Radiance is the physical measurement of the energy radiated from a surface on the earth, usually measured in $\mu W/(cm^2 \bullet nm \bullet sr)$, together with the frequency distribution of that radiation (Canada Centre for Remote Sensing, 2002). The model for radiance is:

$$L_{Sensor}(\lambda) = L_{Sun}(\lambda)\, T(\lambda)\, R(\lambda) + L_{Path}(\lambda)$$

where λ is the wavelength, $L_{Sensor}(\lambda)$ is the radiance at the sensor, $L_{Sun}(\lambda)$ is the solar radiance above the atmosphere, $T(\lambda)$ is the total atmospheric transmittance in the Sun-surface-sensor path, $R(\lambda)$ is the surface reflectance at the observational geometry and $L_{Path}(\lambda)$ is the scattered path radiance (Gao *et al.*, 1991). The radiance is converted to reflectance, which is the ratio of light energy reflected from a surface to the light energy incident on the surface (van der Meer, 2001).

Atmospheric calibration corrects for the geometry of the solar illumination, absorption of the water vapour and gases in the atmosphere, the scattering of particles in the atmosphere as well as the average elevation of the surface of the earth in the image scene (Green, 1991). It is important to identify the appropriate input parameters to the atmospheric correction to ensure the data are accurately representing the atmospheric conditions at the time of image acquisition (Griffin *et al.*, 1999).

The Environment for Visualizing Images (ENVI) Fast Line-of-sight Atmospheric Analysis of Spectral Hypercubes (FLAASH) module, developed by Spectral Sciences, Inc., was used to atmospherically calibrate the AVIRIS data. This program was used to convert the AVIRIS data from radiance to reflectance values based on MODerate resolution TRANsmittance (MODTRAN4) radiative transfer code (Figure 11). MODTRAN4 was developed to improve upon the MODTRAN3 and LOW resolution TRANsmittance (LOWTRAN) atmospheric calibration code to incorporate modifications such as improved ground surface modeling, scattering algorithms and varied spectral resolutions (Berk *et al.*, 1999a).

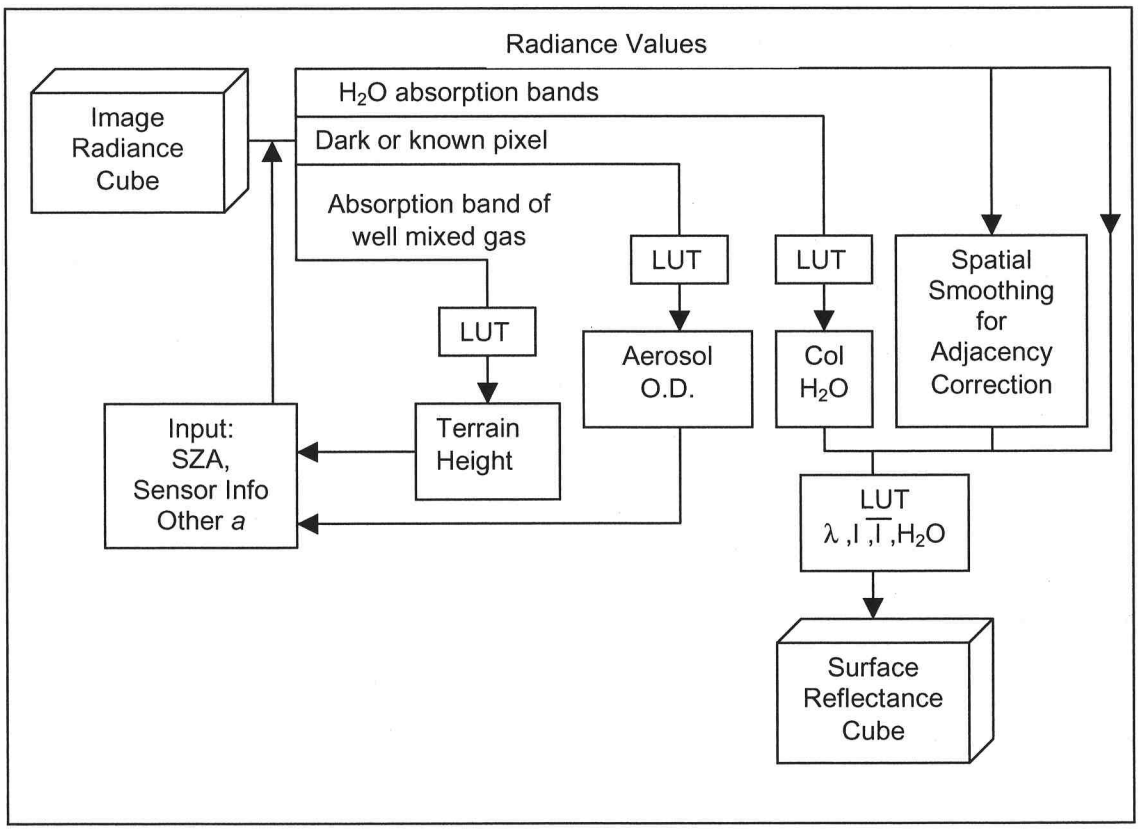

Figure 12: Schematic Flow of FLAASH code
Source: Adapted from Griffin *et al.*, 1999.

To compute the radiance of each wavelength in the AVIRIS data the MODTRAN4 atmospheric code requires solar and viewing geometry, estimates of atmospheric visibility, aerosol model type and atmospheric model (Berk *et al.*, 1999b). The atmospheric model and aerosol type are dependent upon scene characteristics (Adler-Golden *et al.*, 1998). The scene radiance values are then converted to reflectance, using gain, offset and spectral calibration files (see Appendix A for gain, offset and spectral calibration files). Subsequent to atmospheric calibration, the AVIRIS data are prepared for geometric correction.

5.2 Geometric Correction

Geometric correction of the hyperspectral data are performed to allow for variations in the elevation in the GVWD (Dyk *et al.*, 2002). The airborne hyperspectral data are influenced by both systematic and random distortions, including altitude, attitude and sensor velocity (Lillesand and Kiefer, 1994). Prior to receiving the AVIRIS data, a geometric correction, for roll, pitch and yaw, was completed at the Jet Propulsion Laboratory (JPL). Due to the varied elevation in the GVWD, the AVIRIS data were orthocorrected using a 25 metre Digital Elevation Model (DEM), supplied by the British Columbia Ministry of Sustainable Resource Management (MSRM). The orthocorrection was performed in PCI Incorporated image processing software. This process involved collecting Ground Control Points (GCP) using a lake vector, 20 metre and 1 metre orthophotographs using a Thin Plate Spline (TPS) method (Figure 12).

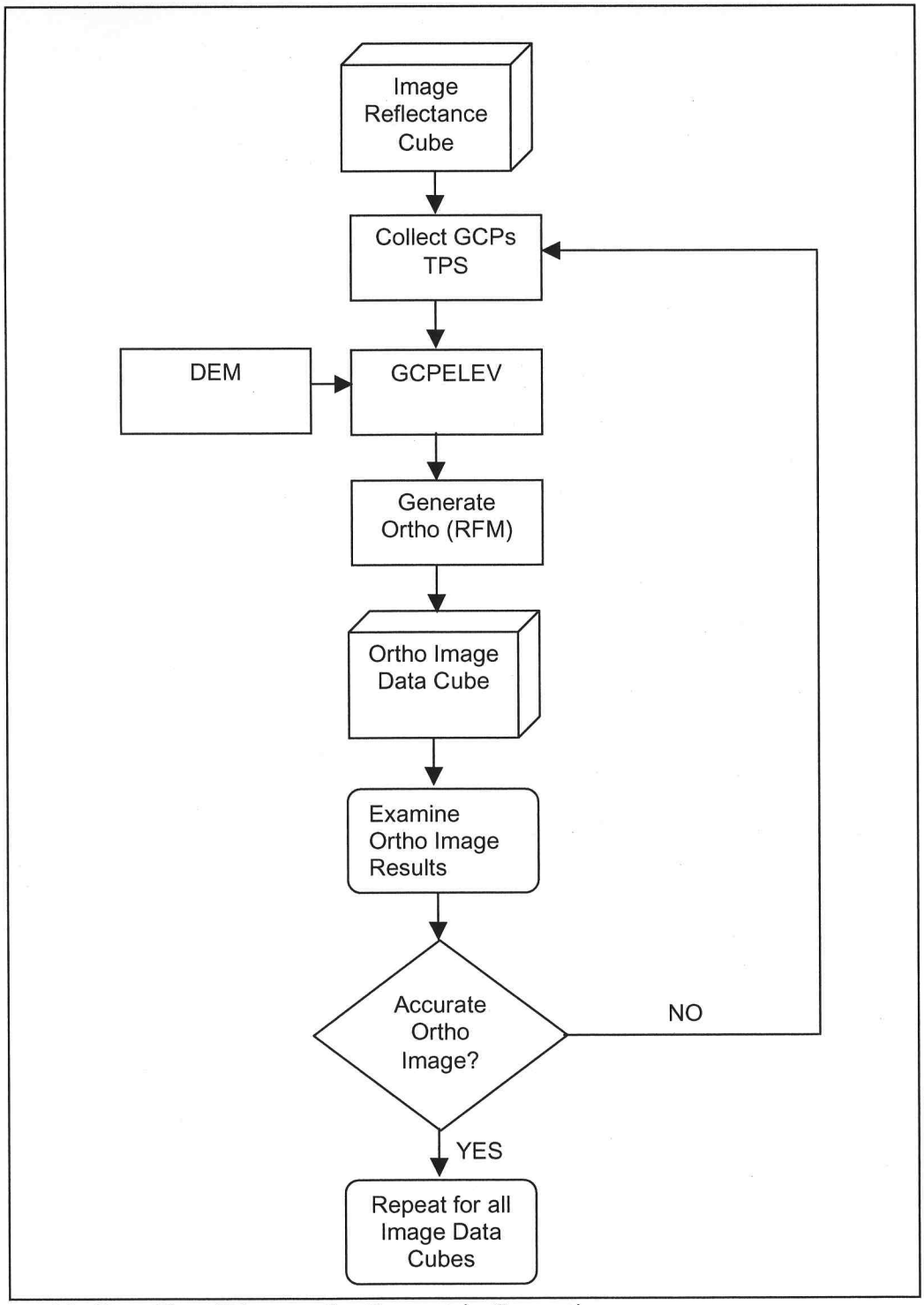

Figure 13: Data Flow Diagram for Geometric Correction

Typically GCPs are collected using a road vector since these features can be easily distinguished in the imagery; however, due to the abundance of lakes and reservoirs in the GVWD, a lake vector was used. These topographical features provide accurate geocorrection because lakes are typically flat regions with little topographic distortion (Dyk et al., 2002).

During GCP collection, the lakes are inversely rubber sheeted to fit the imagery, allowing for more precise collection of GCPs. Each of the six AVIRIS scenes in the GVWD had approximately 40 GCPs collected per scene. One third of the GCPs were used as check points and two thirds were used in the correction for accuracy assessment. Elevation values were obtained using the DEM and recorded with each GCP using the GCPELEV module in PCI. A Rational Function Model (RFM) in PCI Orthoengine, a generalized sensor model that uses the ratios of polynomials, was then applied using the GCPs to orthocorrect the AVIRIS data. A total of six coefficients for the modeling were selected and nearest neighbor resampling was used. This resampling method was used because it did not alter the spectral response of the vegetation. The accuracy of the orthocorrected data was examined using a Root Mean Square (RMS) value. An RMS of half a pixel, in this case 10m, is acceptable. The processed scenes had RMS values of less than 10m. After the AVIRIS data were processed through atmospheric and geometric correction, a spectral calibration was required prior to subsequent analysis.

5.3 Spectral Calibration

An additional correction of the spectra was required, along with the atmospheric and geometric correction of the data (Clark *et al.*, 1993; Aber and Martin, 1995; Kokaly *et al.*,

2003). Image spectral calibration was necessary to ensure that the hyperspectral data reflectance values were similar to the ground spectra for the same target. Calibration of the AVIRIS data was performed using ground spectra acquired by an Analytical Spectrometer Device (ASD). The ASD measurements were acquired at the time of the AVIRIS overflight. Two calibration sites were selected throughout the GVWD, a grassy field (bright target) and a deep-water lake (dark target).

The ground spectra collected from the spectroradiometer were linked to corresponding AVIRIS pixels through the use of GPS data that were acquired at the time of ground spectra collection. This process of spectral calibration is similar to the procedure used by Secker *et al.* (1999). For each image pixel, the corresponding ASD reflectance data were averaged together to calculate a mean ground reflectance. Mean reflectance measurements were used in a weighted average computed from Gaussian curves corresponding to band full width half maximum (FWHM) and centre wavelength for the wavelengths of the AVIRIS data. This process resulted in a binning of 1 nm (2 nm sampling) ground reflectance measurements to 10 nm intervals, which provided a direct comparison between the AVIRIS spectra and the ASD spectra. A force-fit function was created for each pixel at the 437 - 905 nm (VNIR) and 912 - 2365 nm (SWIR) wavelengths by examining the differences in reflectance between the AVIRIS spectra and ground spectra. A function was developed, at the Pacific Forestry Centre, for the entire watershed data and then applied to all six scenes. The spectral calibration process removed any affects on the spectra not modeled by the atmospheric correction.

5.4 Spectral Unmixing

Spectral unmixing was necessary to establish the difference between the reflectance of the forest canopy and that of the forest understory. The forest understory consisted predominantly of salal, which has a higher reflectance in the near infrared than Douglas-fir. In this study the Douglas-fir reflectance is of interest; therefore the quantity of Douglas-fir in each pixel must be known to perform the statistical analysis. The spectral unmixing was used to determine the quantity of Douglas-fir spectra in each of the 20 m hyperspectral pixels in the forested regions of the GVWD. A known spectral comparison method was used in this study to derive the Douglas-fir endmember (Research Systems Incorporated, 2001).

The remote sensing software ENVI was used to determine the quantity of Douglas-fir spectra on a per pixel basis in the AVIRIS data. Prior to the unmixing, a Douglas-fir spectrum was extracted from the AVIRIS data, using a forest mask and an average of the pixels within the forested area. The forest mask was based on a land cover classification of AVIRIS data produced by Goodenough (2003), in which areas classified as Douglas-fir were identified in geocorrected AVIRIS data. A Douglas-fir mask of the identified areas was created and an average of the spectra underneath the mask was used to create a representative spectrum for the unmixing. A mosaic of the six calibrated AVIRIS scenes was used as input to the spectral unmixing. Of the 224 bands in the AVIRIS data, 204 were used in the analysis due to redundant bands and water absorption bands (see Appendix B for AVIRIS channels and wavelengths). The spectral unmixing process in ENVI commences with a computation of a Minimum Noise Fraction (MNF) image,

progresses to an estimation of data dimensionality, requires user supplied endmembers and concludes with a Mixture Tuned Matched Filtering image (Figure 13).

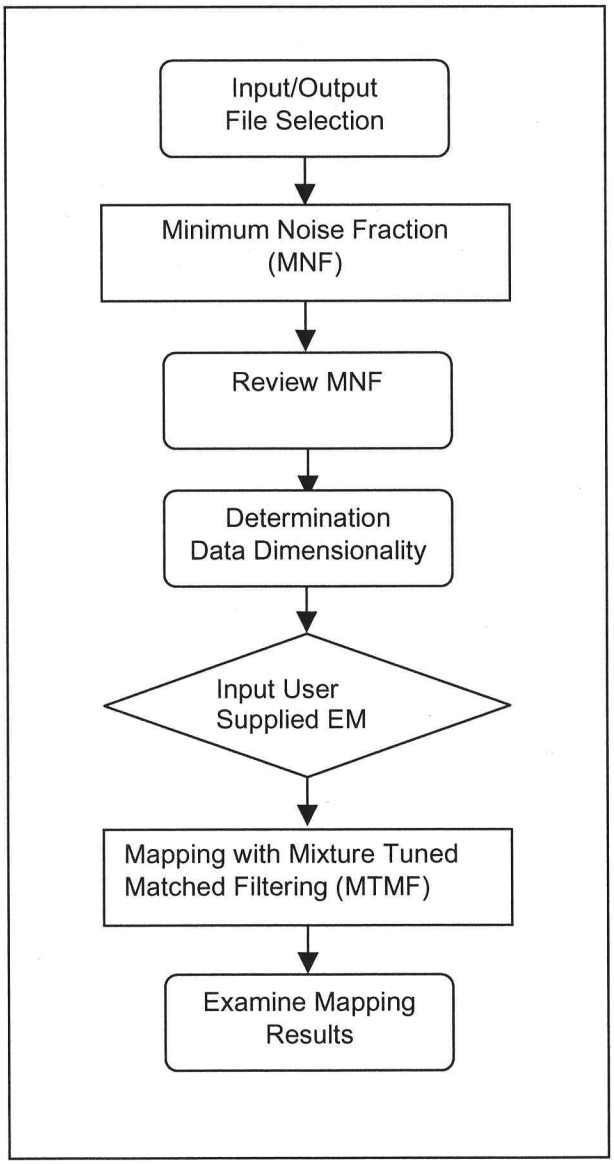

Figure 14: Spectral Unmixing Process Flow Diagram
Adapted from: Research Systems Incorporated, 2001

An MNF transform is a statistical method of determining data redundancy through differentiating between image data and noise inherent in the AVIRIS imagery (Research Systems Incorporated, 2001). A two cascaded Principal Components transform was used

to compute a dataset containing the highest variance in the first few bands and decreasing variance in successive bands until only noise is apparent in the data.

The bands containing valid data are determined by examining both the resulting greyscale MNF bands and the eigenvalues associated with each MNF band. A plot of the eigenvalues and MNF bands is used to determine the appropriate number of MNF bands to use in subsequent analysis. When determining the number of MNF bands to use, it is better to err on the side of caution and use more than the necessary number of bands than to lose data by not choosing enough bands.

The Douglas-fir endmember used in the unmixing was derived from the AVIRIS data, thus providing a more accurate spectrum than that found in a spectral library, since the atmospheric and spectral calibration was applied to the AVIRIS data prior to selecting the Douglas-fir endmember. This endmember was then fed into the MTMF module to determine the endmember fraction for each pixel in the AVIRIS image.

The MTMF results in a grey scale Matched Filter (MF) image with values ranging from 0 to 1, where 0 indicates the lack of endmember present in the pixel and 1 indicates that the pixel is spectrally "pure". Along with the MF image, an infeasibility image, in noise sigma units, was produced to indicate the reliability of the endmember fraction computation. Pixels that are mapped accurately have an MF score above zero and a low infeasibility value (Research Systems Incorporated, 2001), whereas pixels that have a high MF score and a high infeasibility value are considered to be "false positives" and

likely do not represent spectrally pure pixels. A scatterplot of the MF image and the infeasibility image was used to assist in identifying pixels that are spectrally pure. The resulting endmember fractions were then used in the statistical analysis.

5.5 Statistical Analyses

A Partial Least Squares (PLS) regression was used to estimate the biochemical content of the forests in the GVWD employing the calibrated AVIRIS data. This method was adopted to predict an observed dependent variable (the sampled nitrogen, water and total chlorophyll concentrations) from a combination of independent variables (AVIRIS value at each wavelength) using the three-stage regression approach of PLS (Garson, 2002). The PLS method attempts to explain the relationship between the response variation and the predictor variation (SAS, 2001).

PLS regression relies on three main statistical procedures. The first is a principal components regression. A spectral decomposition of $X'X$, where X is the matrix of factors values, is used to explain the maximum amount of variation in the predictor variables. The second procedure is a reduced rank regression where factors are extracted to explain the maximum amount of variation in the response variables. The spectral decomposition of $\hat{Y}'\hat{Y}$, where Y is the matrix of (predicted) response values, is used in this regression. The last procedure is to compute the partial least squares regression, which attempts to explain the relationship between the response and predictor variation, based on a singular value decomposition of $X'Y$. The number of factors extracted from the PLS regression is based on the amount of residual variation in the PLS regression model (SAS, 2001).

The PLS results were computed using SAS statistical software. Input to the PLS procedure included the sampled chemistry data and the AVIRIS spectra at 180 wavelengths in the visible to mid-infrared spectrum (see Appendix C for sample of SAS code). The AVIRIS reflectance data were converted to absorbance and first derivative values as input into the regression.

Absorbance is used to quantify the concentration of energy absorbed by a surface and is computed from the reflectance. The following model was used to calculate absorbance (A):

$$A = \log (1 / R)$$

where R is the reflectance (Wessman *et al.*, 1988).

Derivatives are used to examine the change in slope at each wavelength in a reflectance or absorbance spectrum. A derivative spectrum is used to identify peaks and valleys in the input spectra, highlighting sudden increases or decreases in the spectrum (Smith *et al.*, 2002). It is computed using the bands surrounding a center wavelength that were used as input to a function requiring two matrices, an X matrix (the band wavelengths) and a Y matrix (the value of each pixel). Crammer's Rule was used to calculate the coefficients of the parabola passing through 3 points defined by the (band wavelength, value) points.

The model used to compute the derivatives is:

$$y = 2\,a\,x + b$$

where a and b are the parabola's coefficients calculated by Crammer's Rule and x is the reflectance at a particular wavelength. This was completed using an EASI script developed at the Pacific Forestry Centre (see Appendix D for EASI derivatives script).

Three separate PLS regression models were computed: the first used all twenty-nine Douglas-fir plots, the second used a reduced dataset based on the spectral unmixing results and the third used the reduced dataset as well as the endmember fraction. Each biochemical (nitrogen, total chlorophyll and moisture) was independently modeled.

In each run of the statistical modeling, latent variables were produced using a decomposition of the cross product matrix of the independent and dependent variables. Each latent variable consists of weightings that indicate the contribution of each band number to that latent variable. When computing the latent variables, the goal is to maintain a concentration of information in the first few latent variables (Thermo Galactic, 2002). It is the latent variables that are then used to compute a regression model.

The quality of a PLS regression model is assessed by a cross-validation technique, which can provide an estimate of the error of prediction for a new observation. The objective of this technique is to exclude one sample plot at a time from the analysis and then predict the sample plot chemistry for the excluded plot (SAS, 2001). The predicted residual sum of squares (PRESS) is obtained from this crossvalidation and is used to assess the overall

strength of the regression model. The PRESS is also used as an aide to determine a suitable number of factors to include in the PLS model. A representative model with the fewest number of factors, determined using a PRESS statistic that was not significantly larger than the absolute minimum of PRESS (a saturated model) with the fewest factors, was chosen. Once the appropriate number of factors for a model had been determined, the regression coefficients were extracted for mapping the chemical concentrations.

The statistical significance of the correlation between the dependent (biochemicals) and predictors (AVIRIS spectra by wavelength) was gauged by a t-test of the Fisher-transformed correlation coefficient. The *pwcorr* program in STATA statistical software was used to measure the significance to $p < 0.01$. If ρ is the estimated regression correlation coefficient, the significance (P) of this correlation was (Stata Corporation, 2003, p. 232):

$$\hat{P} = 1\text{-}\mathrm{CDF}_{t,n-2}\left(\frac{\hat{\rho}\times\sqrt{n-2}}{\sqrt{1-\hat{\rho}^2}}\right)$$

where $\mathrm{CDF}_{t,n-2}$ is the cumulative distribution function of Student's t-distribution with n-2 degrees of freedom and n is the number of samples.

To determine the model to be used for biochemical distribution mapping, the significance of each model was assessed using the Akaike Information Criterion (AIC) statistical measure. This statistical measure compensates for the varied number of factors in each model and assesses the models on a common scale.

The following model is used:

$$AIC = n \log (RSS / n) + 2p$$

Where n is the number of samples and p is the number of factors in the model (Venables and Ripley, 1994, p.176).

Finally, the regression models were applied to the AVIRIS data using PCI to produce a distribution map of the predicted biochemical content. Pixel specific AVIRIS data were used as input for the predictions along with the model coefficients at each wavelength. A script developed at the Pacific Forestry Centre was used to apply the regression coefficients to the data (see Appendix E for EASI mapping script).

5.6 Chapter Summary

In order to assess the health of the forest canopy in the GVWD, the hyperspectral remote sensing data were preprocessed and processed to extract estimates of biochemical components. Preprocessing of these data included atmospheric and geometric correction to represent the atmospheric and topographic conditions at the time of image acquisition over the forest canopy. A spectral calibration technique, based on ground spectrometer data, was then applied to the hyperspectral remote sensing data to further correct the airborne spectral measurements. After image preprocessing, the resulting hyperspectral data provided a closer approximation of the energy characteristics of the original scene at the time of image acquisition. The hyperspectral data were then prepared for image processing, which included spectral unmixing and statistical analyses. The following chapter describes the analyses and discussion.

6.0 RESULTS AND DISCUSSION

The following chapter describes the results of the spectral unmixing of the hyperspectral data using ENVI software. The PLS statistical modeling of the hyperspectral and sampled chemistry data is also discussed. Finally, the regional mapping of the GVWD using AVIRIS data is illustrated and discussed.

6.1 Spectral Unmixing

The AVIRIS data were analyzed using a spectral unmixing technique in ENVI image processing software. In order to assess the concentration of Douglas-fir in each AVIRIS pixel, particularly at the plot location, a representative endmember was created. This was done to determine the quantity of Douglas-fir in each pixel by discovering whether the signal found in the hyperspectral data actually indicated Douglas-fir and was not due to other forest species or forest understory species. Regions that were not forested were masked out based on a prior classification (Chen, 2003). These regions were masked because only the forested areas were of interest. Prior to masking the data, the locations of the sample chemistry plots were evaluated to ensure that they fell within the unmixing areas.

Figure 15: AVIRIS mosaic with forest mask

As previously mentioned, a Minimum Noise Fraction (MNF) technique was used to reduce the redundancy in the data set while separating the noise from the useful data. It is well known that the majority of useful data are contained within the first few MNF bands. During the unmixing process, 35 MNF bands were selected for further processing as indicated by the eigenvalues plot (Figure 16). This number is adequate for AVIRIS data because anything beyond 35 bands is considered to be due to noise, as indicated by the

eigenvalues plot where an eigenvalues of 1 indicates noise. The eigenvalue number is the band number of the transformed data, where high eigenvalues indicate a high variance in the MNF data, and thus the presence of useful information. The number of transformed bands is indicated by the change of slope of the eigenvalue curve, and by the eigenvalue dropping to one.

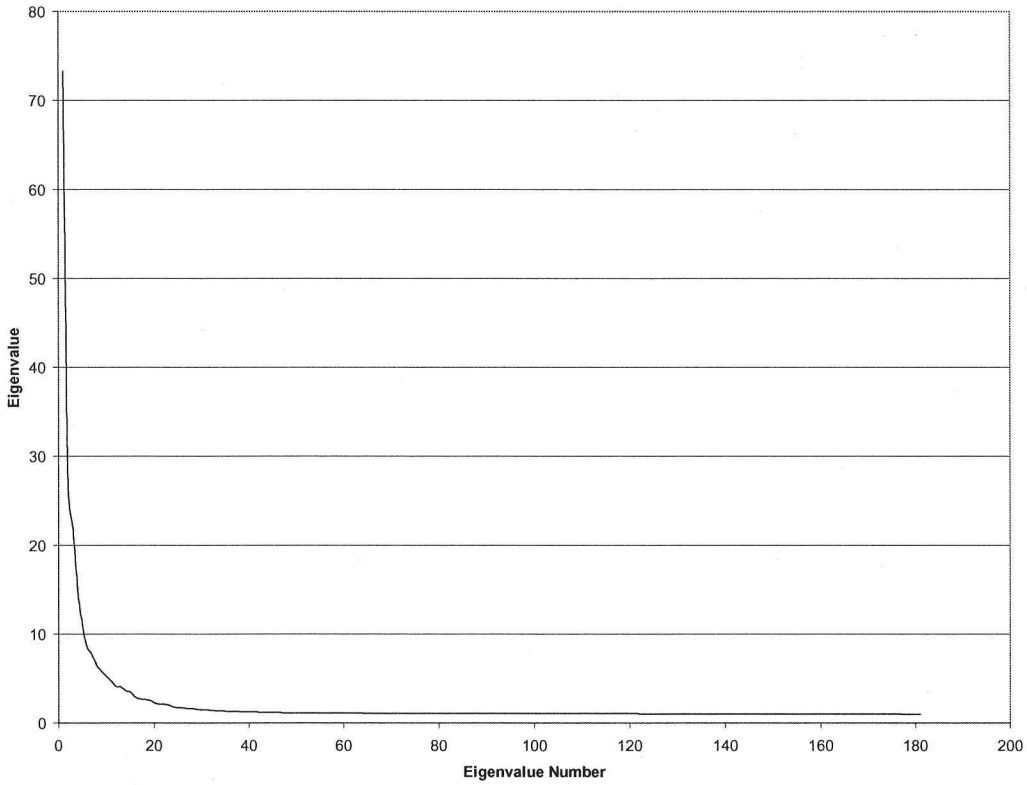

Figure 16: Eigenvalue Plot for MNF

When estimating the number of eigenchannels to use, it is better to overestimate than to underestimate, otherwise valuable information can be lost.

The Douglas-fir endmember spectra (Figure 17) were used to determine the composition of each pixel in the masked image.

Figure 17: Douglas-fir input spectra

With the spectral input, a Mixture-Tuned Matched Filtering (MTMF) was used to map the endmember (Figure 18). The MTMF process is used to compute the endmember fraction in each image pixel. The result of the MTMF is a 32-bit greyscale image indicating the fraction of the input endmember spectra. Along with the MTMF image is an infeasibility image, which is also a 32-bit greyscale image showing the likelihood of the pixel being correctly classified.

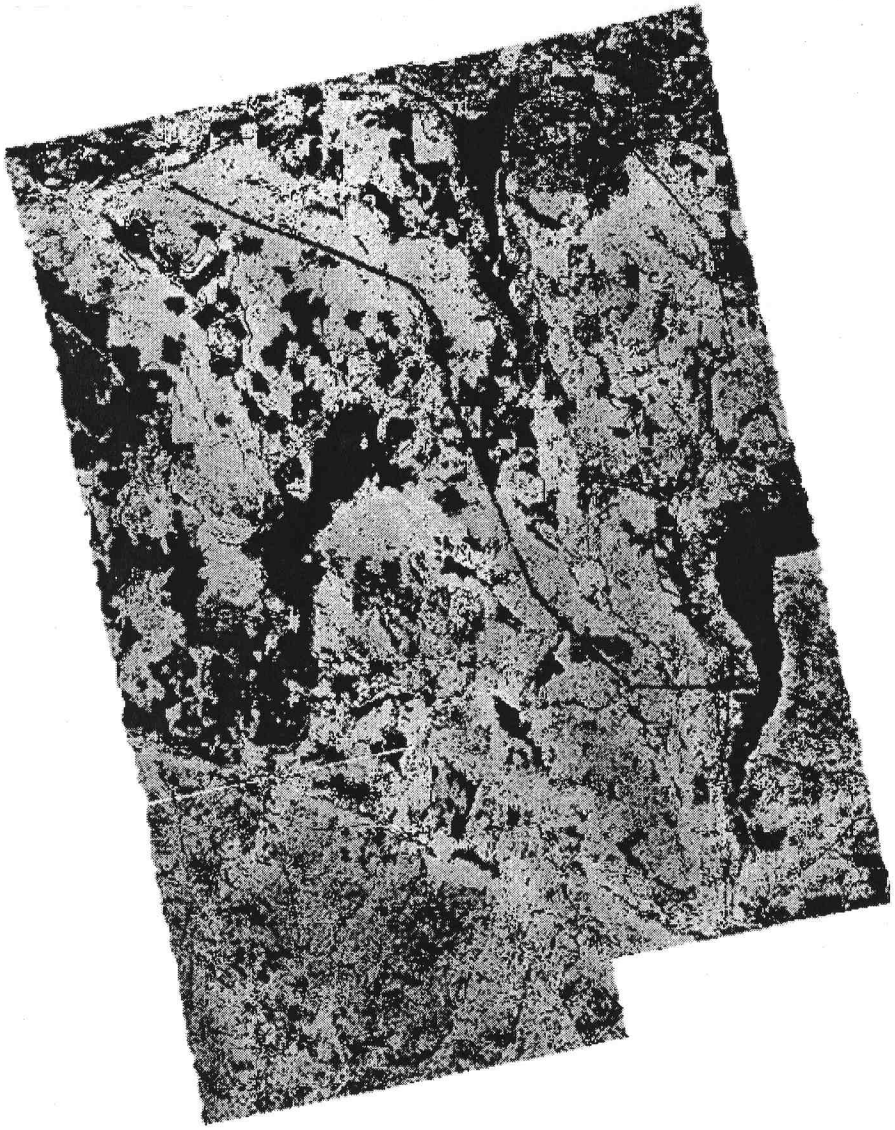

Figure 18: MTMF image with forest mask

As previously mentioned, the MTMF image along with the infeasibility image are used to determine pixels that contain Douglas-fir spectra. Inherent in the MTMF method is the possibility of "false positives" where the endmember spectra are incorrectly identified. The infeasibility image can be used to determine pixels that have been falsely identified as the input endmember spectra, where a high infeasibility indicates a false endmember prediction. Pixels that have been identified as containing Douglas-fir spectra and have a low infeasibility value are considered to be true.

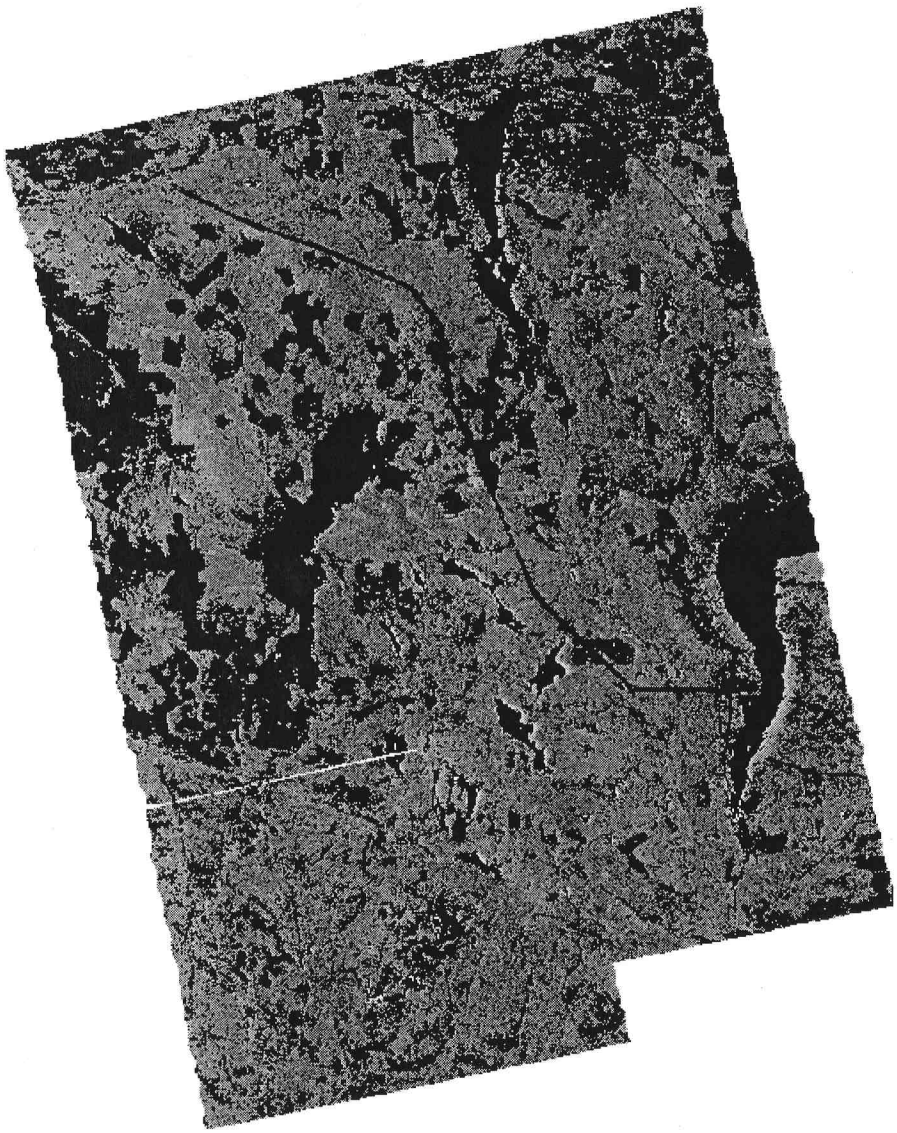

Figure 19: Infeasibility Image with forest mask

Results of the spectral unmixing indicated that six out of 29 plots did not have a significant endmember fraction of Douglas-fir spectra (Table 2). The twenty-three remaining plots were then used in a dataset for the statistical modeling.

Table 2: Spectral Unmixing results

Plot Number	Endmember Average	Endmember Standard Deviation
1	0.0264	0.0224
2	0.0000	0.0000
5	0.1228	0.0173
7	0.4658	0.0187
8	0.1587	0.0141
9	0.0228	0.0219
10	0.1986	0.0278
13	0.0773	0.0198
14	0.1930	0.0183
17	0.3122	0.0199
19	0.2721	0.0301
24	0.0000	0.0000
25	0.0000	0.0000
29	0.0000	0.0000
30	0.1114	0.0143
31	0.1821	0.0226
32	0.0000	0.0000
33	0.0114	0.0324
34	0.0000	0.0000
44	0.3380	0.0137
45	0.3873	0.0204
46	0.3295	0.0260
47	0.6560	0.0195
48	0.5028	0.0153
49	0.4581	0.0164
50	0.4013	0.0217
51	0.1545	0.0139
52	0.5906	0.0164
53	0.1685	0.0329

Although ENVI is the only commercial software available to perform the spectral unmixing, it has been noted that this is not the ideal method of unmixing for vegetation studies due to the method of representative endmember selection. The unmixing does allow for the examination of the composition of the AVIRIS pixels at each plot and is used to eliminate plots that do not have any Douglas-fir components. Plots that contain

Douglas-fir spectra can then be used for the statistical modeling of the biochemistry in the GVWD.

6.2 Statistical Modeling

In order to determine the biochemical distribution of the GVWD, a PLS regression was used to model the biochemistry. As previously mentioned, the PLS regression is an Multivariate Linear Regression (MLR) with the following assumptions (Hair *et al.*, 2002):

1. The data can be described in a statistical relationship.
2. The data are approximately normally distributed.
3. There is an equal variance of the criterion variable.
4. There must be a lack of correlation errors in the data.
5. The data relationship can be described in linear manner.
6. There must be a constant variance of the error term.
7. Lastly, the data are independent observations collected in a random manner.

The data used in this study were examined to assure these assumptions were met. Both the dependent and independent variables were inspected to ensure the distributions were normal and that an absence of multicollinearity - when the relationship between two or more independent variables exhibits a high correlation (Hair *et al.*, 1992) - existed. With regards to the assumptions of PLS regression modeling, MLR assumptions must be met particularly the absence of outliers in the data (Galadi and Kowalski, 1986).

The PLS method of MLR modeling is preferred over other methods, specifically Stepwise Multiple Regression, because it allows for the modeling of multiple dependent as well as independent variables. The inclusion of the Principal Components Regression (PCR) allows for the issue of multicollinearity to be addressed through the creation of latent variables that are not correlated which are used in the PLS regression; this step of the PLS process also can be used to reduce data noise (SAS, 2001). This is of particular importance in this study, since multicollinearity among the independent variables is evident. While PLS regression cannot be used to interpret the underlying relationships between the independent variables, it can be used as a predicted technique (Garson, 2002).

Validity, defined as "the ability of a construct's indicators to measure the concept under study accurately (Hair *et al.*, 1992, 431)", of the model is performed to ensure that the general population is indeed represented by the model. The term validity is separate from the term reliability, the consistency of a model; however, these two concepts are related (Hair *et al.*, 1992). In other words, a model can be valid and yet not reliable or accurate.

The cross-validation option used during the modeling was one-at-a-time cross-validation. This method of cross-validation excludes one plot at a time to predict the biochemical measurement; the plot is then re-entered into the regression until all plots have been cycled through; finally the best model for the dataset is computed. The Predicted Residual Sum of Squares (PRESS) statistic was used to determine the appropriate number

of factors for each model, where the PRESS statistic that was significantly different from the absolute minimum PRESS value is selected.

Three datasets were used in the PLS; these were selected based on the spectral unmixing results: the first contained the full dataset of 29 plots; the second contained a subset of the full dataset based on the spectral unmixing results with 23 plots; the third also contained a subset of the full dataset based on the spectral unmixing results with 23 plots but in addition included the spectral component of the Douglas-fir as a dependent variable. Within each dataset, each biochemical - nitrogen, total chlorophyll and moisture - was modeled separately.

6.2.1 Nitrogen

Table 3 shows the coefficient of determination (r^2) for each test, where Full was the full dataset, Subset was the subset based on the spectral unmixing and Endmember was the subset based on the spectral unmixing and the endmember fraction when modeling nitrogen. The r^2 value was used to indicate the total variation of the dependent variables that can be attributed to the relationship with the independent variables.

The Factors column indicated the number of factors required for the model. The factors created during the PLS modeling have not been examined to determine if indeed they correspond to features on the ground or climatic variables. The model with the least number of variables with a high coefficient represents the model of choice; the models that are highlighted indicate the models of choice within each dataset. At times, there was no model of choice, as indicated in Subset row of Table 3. When selecting a model, a

decision to use fewer factors with lower coefficient of determination values was warranted to avoid overfitting of the dataset.

Table 3: Nitrogen Coefficient of Determination for PLS regression

Dataset	Factors	Reflectance	Factors	Absorbance	Factors	Absorbance First Derivative
Full	15	0.9990*	12	0.9874*	**5**	**0.8246***
Subset	14	0.2002	13	0.1974	2	0
Endmember	5	0.6875*	15	0.9972*	**8**	**0.8770***

The * indicates a significant relationship.

The r^2 of both the full dataset and the endmember datasets, when using the first derivative of the absorbance, were deemed to be adequate regression models due to the significance of the models and the number of factors used in the modeling. The progression of the increase in r^2 values demonstrates that when taking into consideration the endmember fraction of the plots, the total variation of the dependent variables that can be attributed to the relationship with the independent variables increases.

The significance of each model within the dataset used (Full, Subset and Endmember) was measured to determine which model provided the most appropriate model for nitrogen. The AIC statistic was computed to account for differences in the number of factors used in each regression model and is similar to ranking system. Typically the lower AIC values indicated the model to use; however, in some cases if the AIC values were similar, either model could be used. Both the full and endmember datasets had lower AIC values than the subset dataset, and could indicate appropriate models (Table 4).

Table 4: Nitrogen AIC

Dataset	Reflectance	Absorbance	Absorbance First Derivative
Full	30.004	24.004	**10.005**
Subset	28.005	26.008	4.007
Endmember	10.005	30.005	**16.009**

6.2.2 Total Chlorophyll

The PLS results indicate that when using the full dataset, an r^2 of 0.43 was achieved when using the reflectance values, the r^2 of the subset dataset was 0.50 when using the absorbance and the r^2 of the endmember dataset was 0.73 when using the first derivatives of the absorbance (Table 5). The increase in r^2 from the full dataset to the endmember dataset show that when knowing the composition of the pixel, specifically the Douglas-fir components, the total variation of the dependent variables that could be attributed to the relationship with the independent variables increases.

Table 5: Total Chlorophyll Coefficient of Determination for PLS regression

Dataset	Factors	Reflectance	Factors	Absorbance	Factors	Absorbance First Derivative
Full	**4**	**0.4307***	15	0.9984*	15	0.9998*
Subset	4	0.4641*	**4**	**0.5009***	1	0.0000
Endmember	5	0.4648*	15	0.9930*	**6**	**0.7331***

The * indicates a significant relationship.

The AIC values were computed for each regression model (Table 6). Results indicated that when the full dataset and reflectance were used, the AIC was the lowest. The lowest AIC in the subset dataset did not correspond to the significant model. In the endmember subset both the reflectance and first derivatives of the absorbance have how lower AIC values then the absorbance, which could indicate appropriate models.

Table 6: Total Chlorophyll AIC

Dataset	Reflectance	Absorbance	Absorbance First Derivative
Full	**8.004**	30.005	30.005
Subset	8.004	8.007	2.007
Endmember	10.005	30.000	**12.006**

6.2.3 Moisture

When modeling moisture, only one significant relationship was found with an r^2 value of 0.32 (Table 7). The lack of more significant relationships could to be due to the difficulty in estimating moisture from hyperspectral data or perhaps the methods used to estimate the moisture.

Table 7: Moisture Coefficient of Determination for PLS regression

Dataset	Factors	Reflectance	Factors	Absorbance	Factors	Absorbance First Derivative
Full	3	0.1472	**4**	**0.3200***	2	0.1924
Subset	3	0.1486	2	0.1601	2	0.2520
Endmember	3	0.1486	2	0.1600	2	0.2520

The * indicates a significant relationship.

The AIC value for the only significant relationship in the moisture modeling did not have the lowest AIC value which can indicate that the model was not appropriate for predicting moisture using this particular set of plots (Table 8).

Table 8: Moisture AIC

Dataset	Reflectance	Absorbance	Absorbance First Derivative
Full	6.494	8.494	4.533
Subset	6.646	4.660	4.626
Endmember	6.580	4.580	4.626

It is important to the note that regression modeling of biochemicals in the GVWD is a complex issue where there is no absolute model that can be computed to estimate the

regional distribution of biochemistry in the watershed. That is to say that if the models were to be computed with the inclusion of the other data plots, the models may evolve.

6.3 Mapping

One of the objectives of this research was to determine if the AVIRIS data could be used to map the distribution of the biochemicals in the GVWD on a regional scale. The spectral unmixing and statistical modeling of the AVIRIS data were used as input for nitrogen and total chlorophyll mapping in the GVWD. Through the statistical analysis it was determined that it is difficult to estimate moisture concentrations given the nature of the methods used and the sensitivity to moisture in the atmosphere; therefore, moisture mapping was not attempted.

Using a script developed at the Pacific Forestry Centre, both nitrogen and total chlorophyll concentrations in the GVWD were mapped. The best regression model for each biochemical was used as input for the mapping script; for both nitrogen and total chlorophyll the first derivatives of the absorbance were used as input for the distribution maps. The mapping script uses the offset and coefficients computed from the PLS regression and applies them to the Douglas-fir areas in AVIRIS data, as determined by the mask. Figure 20 illustrates the nitrogen concentration throughout the forested regions of the GVWD.

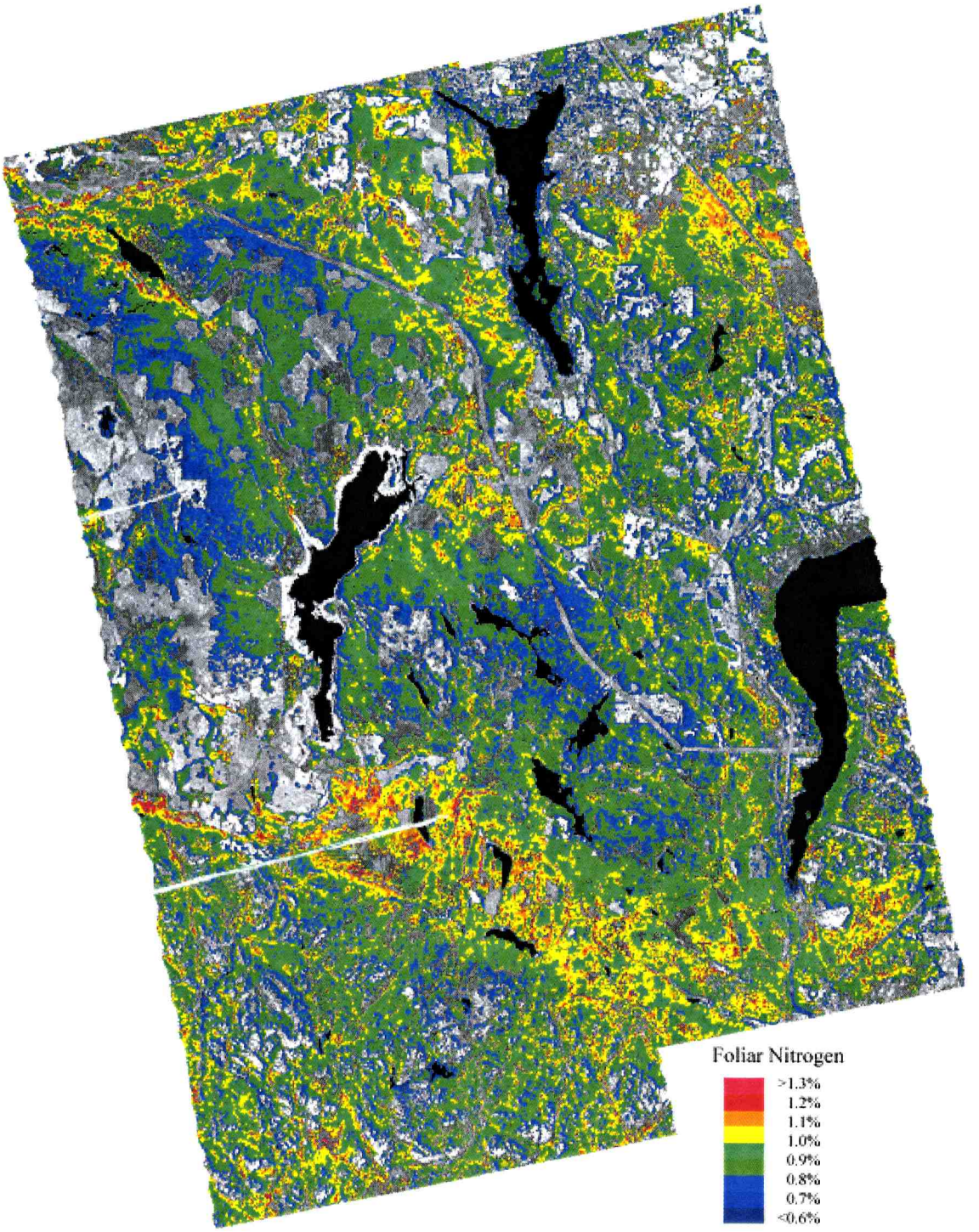

Figure 20: GVWD Nitrogen Map

Figure 21 illustrates the total chlorophyll concentration throughout the forested regions of the GVWD.

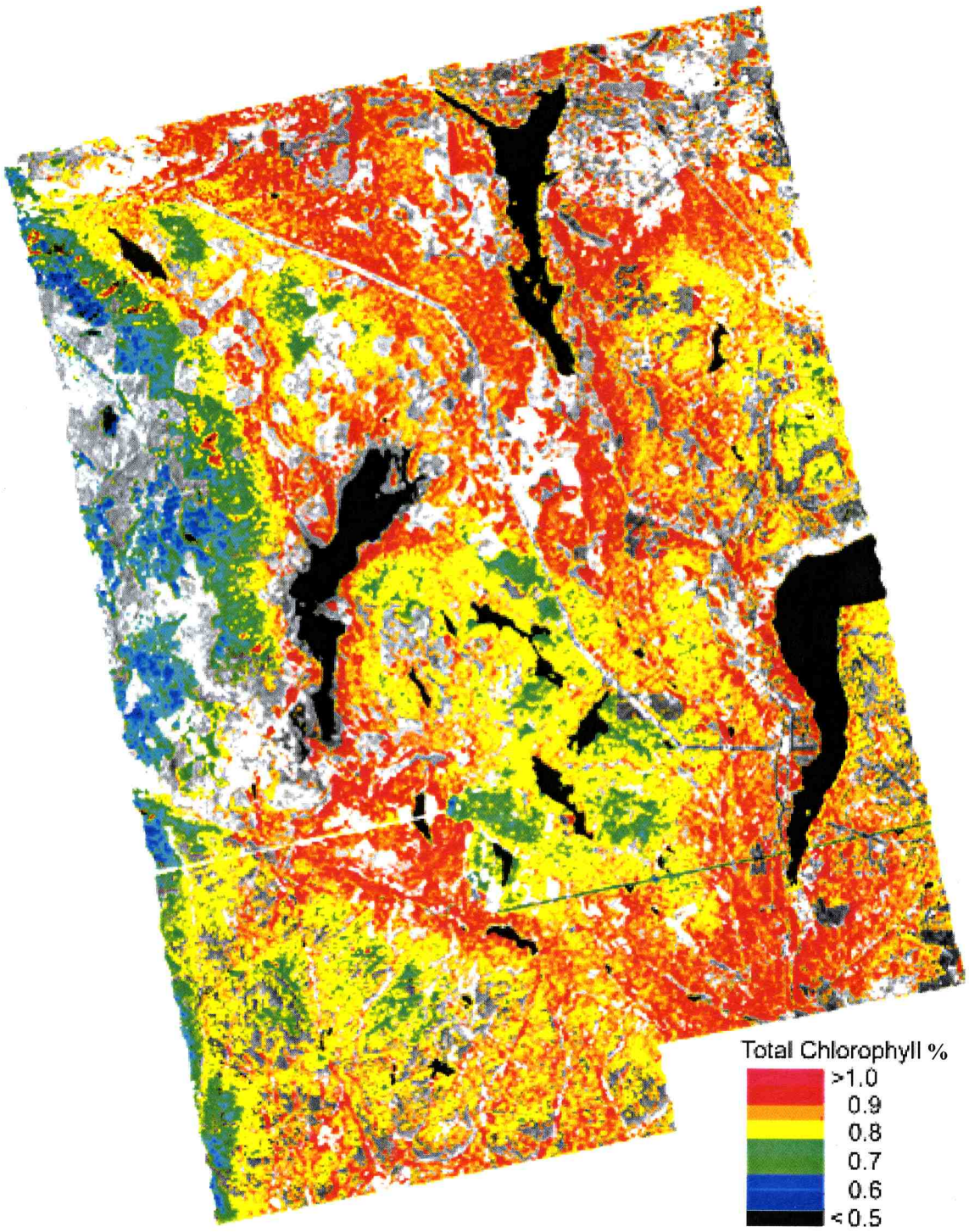

Figure 21: GVWD Total Chlorophyll Map

While the models that were selected for use in the mapping of the biochemical distributions were validated, it is important to note that the reliability of the mapping is

difficult to assess. The goal of regression modeling is to develop a model that can be used to map the distribution, however, this may or may not correspond to the conditions in the entire GVWD, specifically in the Douglas-fir forested regions. While this is true, the data plots that were used in the modeling can be commented on in terms of statistical significance and used as a predictive, rather than interpretive means.

Each of the biochemicals examined in this study is essential for tree growth and development. The presence or absence of specific biochemicals can determine forest conditions. Nitrogen is an important chemical in forest growth and development; measures of total chlorophyll and moisture concentration can be used to estimate the overall canopy health.

6.4 Chapter Summary

Methods used to map the distribution of biochemistry of the GVWD were examined in this chapter. Through spectral unmixing and statistical modeling, the distribution of nitrogen and total chlorophyll in the watershed were mapped. Due to limitations of the hyperspectral data, the distribution of moisture was unable to be mapped. Spectral unmixing provided a method of extracting Douglas-fir concentrations in the AVIRIS data, based on sampled chemistry data. Statistical models provided direct input into the mapping procedure, with r^2 of 0.73 for nitrogen and 0.68 for total chlorophyll. Conclusions based on the analysis and discussion of the research and opportunities for further investigation are discussed in the Chapter 7.

7.0 CONCLUSIONS

In the following section conclusions obtained from the research, limitations of the data and methods, and recommendations for future research are provided.

7.1 Conclusions

The ability to examine vegetation biochemistry from an airborne platform is valuable because it provides a comprehensive view of the forested environments of Canada. Understanding the biochemistry of forests allows for insight into ecosystem processes such as photosynthesis and nutrient cycling. With the capability to provide high spectral information about the forest, the hyperspectral airborne sensor AVIRIS offers a means of examining biochemicals.

The GVWD is an ideal study site for hyperspectral remote sensing of vegetation biochemistry due to the availably of airborne hyperspectral data, field spectrometer measurements and field chemistry samples. Information contained within the hyperspectral data were examined through spectral unmixing and statistical methods that provided a means of examining the value of AVIRIS hyperspectral data for estimating the distribution of biochemicals in the GVWD. The spectral unmixing of the imagery assisted in determining the composition of each pixel in the AVIRIS data and improving statistical modeling of the biochemicals. In performing the spectral unmixing, a method of differentiating the understory from the forest canopy, specifically the Douglas-fir canopy, was achieved. The results of the unmixing were used to provide input into three different regression models for each biochemical.

The PLS regression was used to model the distribution of the biochemicals based on the field sampled chemistry data. PLS results indicate that nitrogen and total chlorophyll correlation coefficients improve as the dataset is refined with the spectral unmixing results. Nitrogen and total chlorophyll r^2 values are 0.73 and 0.68 respectively. Due to the complexity of moisture interaction with hyperspectral data, regression models were unable to be computed for the AVIRIS data over the GVWD. Regression models were then applied to the entire AVIRIS dataset for regional mapping of the canopy biochemistry. The distribution of nitrogen and total chlorophyll in the forested areas of the GVWD were mapped.

Others have used the methods investigated in this research; however, not many studies have been conducted on Coastal Douglas-fir tree species to estimate biochemistry and to map on a regional level. The methods used in this research could be used by other researchers who are attempting to estimate biochemistry in conifer species in similar ecosystems. The application of nitrogen and total chlorophyll mapping on a regional basis allows for input into forest management practices.

7.2 Recommendations

To further improve upon the methods for determining canopy biochemical distribution in the GVWD, the following recommendations hold true. It is important to correlate the AVIRIS data acquisition and field spectrometer data acquisition with the chemistry sampling. This will provide an accurate assessment of the biochemistry at the time of image acquisition and perhaps further improve modeling results.

The method of spectral unmixing in this research was not ideal for vegetated environments, where other methods of unmixing may provide a more in-depth and appropriate method of pixel decomposition. This research utilized a known spectral endmember analysis; perhaps deriving the endmembers directly from the image scenes may yield improved results.

The statistical modeling of these data can be approached using different methods than that employed here. Although this method of statistical analysis provided adequate results, a process of band correlations prior to regression analysis could be used to determine spectral wavelengths that are correlated and focus on absorption bands that provide more information than those used in this research.

REFERENCES

Aber, J. and M. Martin, 1995. High spectral resolution remote sensing of canopy chemistry, Jet Propulsion Laboratory (JPL) AVIRIS Workshop, Pasadena, California, pp. 1-4.

Adler-Golden, S., A. Berk, S. Richtsmeier, P. Acharya, M. Matthew, G. Anderson, C. Allred, L. Jeong and H. Chetwynd, 1998. FLAASH, A MODTRAN4 atmospheric correction package for hyperspectral data retrievals and simulations, Jet Propulsion Laboratory (JPL) AVIRIS Workshop, Pasadena, California, USA, pp. 1-6.

Ahern, F., 1988. The effects of bark beetle stress on foliar spectral reflectance of lodgepole pine. International Journal of Remote Sensing, 9(9): 1451-1468.

Apple, M., K. Tiekotter, M. Snow, J. Young, A. Soeldner, D. Phillips, D. Tingey and B. Bond, 2002. Needle anatomy changes with increasing tree age in Douglas-fir. Tree Physiology, 22: 129-136.

Banninger, C., 1989. Mapping stress-related biochemical changes in coniferous forests with airborne imaging spectrometer (AIS-2) data, 9th EARSeL Symposium, Espoo, pp. 512-518.

Berk, A., G. Anderson, P. Acharya, J. Chetwynd, L. Bernstein, E. Shettle, M. Matthew and S. Adler-Golden, 1999. MODTRAN4 Version 2 User's Manual, Air Force Research Laboratory, Maryland.

British Columbia Ministry of Forests, 1991. Ecosystems of British Columbia, Victoria, British Columbia.

Brix, H., 1992. Fertilization and thinning effect on a Douglas-fir ecosystem at Shawnigan Lake: A synthesis of project results. FRDA 196, Victoria.

Broge, N. and E. Leblanc, 2000. Comparing prediction power and stability of broadband and hyperspectral vegetation indices for estimation of green leaf area index and canopy chlorophyll density. Remote Sensing of Environment, 76: 156-172.

Caetano, M., T. Oliveira, J. Paul, M. Vasconcelos and J. Pereira, 1997. Mapping shrublands and forests with multispectral satellite images based on spectral unmixing of scene components. SPIE, 3222: 4-14.

Canada Centre for Remote Sensing, 2002. Glossary of Remote Sensing Terms. Natural Resources Canada.

Canada Centre for Remote Sensing, 2003. Fundamentals of Remote Sensing. Canada Centre for Remote Sensing.

Canadian Forest Service, 2002. State of Canada's Forests 2001-2002, Natural Resources Canada, Ottawa.

Capital Regional District, 2003. 2003 Greater Victoria Water Supply Area. Capital Regional District, Victoria, British Columbia.

Chabrillat, S., P. Pinet, G. Ceuleneer, P. Jonhson and J. Mustard, 2000. Ronda peridotite massif: methodology for its geological mapping and lithological discrimination from airborne hyperspectral data. International Journal of Remote Sensing, 21(12): 2363-2388.

Chapin, F., 1980. The mineral nutrition of wild plants. Annual Review of Ecology and Systematics, 11: 233-260.

Chatterjee, S., A. Hadi and B. Price, 2000. Regression Analysis by Example. John Wiley & Sons, Incorporated, Toronto, 359 pp.

Chen, H., 2003. An Advanced Classification System for Processing Multitemporal Landsat Imagery and Producing Kyoto Protocol Products. Master's Thesis, Department of Computer Science, University of Victoria, Victoria, British Columbia.

Clark, R., G. Swayze, K. Heidebrecht, A. Geotz and R. Green, 1993. Comparison of methods for calibrating AVIRIS data to ground reflectance, Jet Propulsion Laboratory (JPL) AVIRIS Workshop, Pasadena, California, USA, pp. 35-36.

Clark, R., G. Swayze, E. Livo, R. Kokaly, T. King, B. Dalton, S. Vance, B. Rockwell, T. Hoefen and R. McDougal, 2002. Surface reflectance calibration of terrestrial imaging spectroscopy data: a tutorial using AVIRIS, Jet Propulsion Laboratory (JPL) AVIRIS Workshop, Pasadena, California, USA.

Clark, R. and T. Roush, 1984. Reflectance spectroscopy: quantitative analysis techniques for remote sensing applications. Journal of Geophysical Research, 89: 6329-6340.

Clevers, J. and R.J Jongschaap, 2001. Imaging Spectrometry for Agricultural Applications. In: F.a.S.d.J. van der Meer (Editor), Imaging Spectrometry. Kluwer Academic Publishers, Dordrecht, Netherlands, pp. 157-199.

Cudahy, T., T. Hewson, J. Huntington, M. Quigley and P. Barry, 2001. The performance of the satellite-borne Hyperion hyperspectral VNIR-SWIR imaging system for mineral mapping at Mount Fitton, South Australia, International Conference on Geoscience and Remote Sensing, Sydney, Australia.

Curran, P., 1989. Remote sensing of foliar chemistry. Remote Sensing of Environment, 30: 271-278.

Curran, P., J. Dungan, B. Macler, S. Plummer and D. Peterson, 1992. Reflectance spectroscopy of fresh whole leaves for the estimation of chemical concentration. Remote Sensing of Environment, 39: 153-166.

Curran, P., J. Kupiek and G. Smith, 1997. Remote sensing the biochemical compositions of a slash pine canopy. IEEE Transactions on Geoscience and Remote Sensing, 35(2): 415-420.

Curran, P., Dungan, J. and D. Peterson, 2001. Estimating the foliar biochemical concentration of leaves with reflectance spectrometry - testing the Koklay and Clark methodologies. Remote Sensing of Environment, 76: 349-359.

Daughtry, C., C. Walthall, M. Kim, E. brown de Colstoun and J. McMurtrey III, 2000. Estimating corn leaf chlorophyll concentration from leaf and canopy reflectance. Remote Sensing of Environment, 74: 229-239.

Dyk, A., D. G. Goodenough, A. S. Bhogal, J. Pearlman and J. Love, 2002. Geometric correction and validation of Hyperion and ALI data for EVEOSD, International Geoscience and Remote Sensing Symposium, Toronto, Ontario, Canada, pp. 579-583.

Gao, B., A. Goetz and J. Zamudio, 1991. Removing atmospheric effects from AVIRIS data for surface reflectance retrievals, Jet Propulsion Laboratory (JPL) AVIRIS Workshop, Pasadena, California, USA, pp. 80-86.

Gao, B. and A.Goetz, 1995. Retrieval of equivalent water thickness and information related to biochemical components of vegetation canopies from AVIRIS data. Remote Sensing of Environment, 52: 155-162.

Garson, J., 2002. Quantitative Methods in Public Administration. http://www2.chass.ncsu.edu/garson/pa765/statnote.htm

Gastellu-Etchgorry, J., F. Zagolski, E. Mougin, G.Marty and G. Giordano, 1995. An assessment of canopy chemistry with AVIRIS - a case study in the Landes Forest, South-west France. International Journal of Remote Sensing, 16(3): 487-501.

Gausman, H.and J. Quisenberry, 1990. Spectrophotometric detection of plant leaf stress. In: F. Katterman (Editor), Environmental Injury to Plants. Academic Press, Inc., Toronto, pp. 257-280.

Geladi, P. and B. Kowalski, 1986. Partial least-squares regression: a tutorial. Analytical Chimica Acta, 185: 1-17.

Gong, P., R. Pu and B. Yu, 1997. Conifer species recognition: an exploratory analysis of in situ hyperspectral data. Remote Sensing of Environment, 62: 189-200.

Goodenough, D., A. Bhogal, A. Dyk, O. Niemann, T. Han, H. Chen, C. West and C. Schmidt, 2001. Calibration of forest chemistry for hyperspectral analysis, International Geoscience And Remote Sensing Symposium 2001, Sydney, Australia, pp. 52-56.

Goodenough, D.G., A. Dyk, K. O. Niemann, J. Pearlman, H. Chen, T. Han, M. Murdoch and C. West, 2003. Processing Hyperion and ALI for forest application. IEEE Transactions on Geoscience and Remote Sensing, 41(6): 1321-1331.

Goodenough, D.G., H. Chen, A. Dyk, T. Han, S. McDonald, M. Murdoch and C. West, 2003. 2003. Forest Information Products from AVIRIS and Hyperion, Jet Propulsion Laboratory (JPL) AVIRIS Workshop, Pasadena, California, USA.

Green, R., G. Vane and J. Conel, 1988. Determination of in-flight AVIRIS spectral, radiometric, spatial and signal-to-noise characteristics using atmospheric and surface measurements from the vicinity of the rare-earth-bearing carbonatite at Mountain Pass, California, Jet Propulsion Laboratory (JPL) AVIRIS Workshop.

Green, R., S. Larson and H. Novack, 1991. Calibration of AVIRIS digitized data, Jet Propulsion Laboratory (JPL) AVIRIS Workshop, Pasadena, California, USA.

Griffin, M., H. Burke, J. Vail, S. Adler-Golden and M. Matthew, 1999. Sensitivity of atmospheric compensation model retrievals to input parameter specification, Jet Propulsion Laboratory (JPL) AVIRIS Workshop, Pasadena, California, USA.

Hair, J., Anderson, R., Tatham, R. and W. Black, 1992. Multivariate data analysis with Readings. Macmillan Publishing Company, New York, New York, USA.

Hall, A., 1957. An Introduction to Forest Soils of the Douglas-fir Region of the Pacific Northwest, Hall, Anderson, Seattle.

Holden, H. and E. LeDrew, 2001. Hyperspectral discrimination of healthy versus stressed corals using in situ reflectance. Journal of Coastal Research, 17(4): 850-858.

Hurcom, S., A. Harrison, and M. Taberner, 1996. Assessment of biophysical vegetation properties through spectral decomposition techniques. Remote Sensing of Environment, 56: 203-214.

Jensen, J., 1996. Introductory Digital Image Processing: A Remote Sensing Perspective. Prentice Hall, Upper Saddle River, New Jersey, USA.

Jensen, J., 2000. Remote Sensing of the Environment. Prentice Hall, Upper Saddle River, New Jersey, USA.

Johnson, L. and C. Billow, 1996. Spectrometric estimation of total nitrogen concentration in Douglas-fir foliage. International Journal of Remote Sensing, 17(3): 489-500.

Knipling, E., 1970. Physical and physiological basis for the reflectance of visible and near-infrared radiation from vegetation. Remote Sensing of Environment, 1: 155-159.

Kokaly, R., 2000. Investigating a physical basis for spectroscopic estimates of leaf nitrogen concentration. Remote Sensing of Environment, 75(2): 153-161.

Kokaly, R., D. Despain, R. Clark and E. Livo, 2003. Mapping vegetation in Yellowstone National Park using spectral feature analysis of AVIRIS data. Remote Sensing of Environment, 84: 437-456.

Kokaly, R. and R. Clark, 1999. Spectroscopic determination of leaf biochemistry using band-depth analysis of absorption features and stepwise multiple linear regression. Remote Sensing of Environment, 67: 267-287.

Kramer, P. and T. Kozlowski, 1979. Physiology of Woody Plants. Academic Press, Incorporated, Toronto.

Kruse, F., A. Lefkoff and J. Dietz, 1993. Expert system-based mineral mapping in Northern Death Valley, California/Nevada, using Airborne Visible/Infrared Imaging Spectrometer (AVIRIS). Remote Sensing of Environment, 44: 309-336.

Kruse, F., 1997. Regional geologic mapping along the Colorado Front Range from Ft Collins to Denver using the Airborne Visible/Infrared Imaging Spectrometer (AVIRIS), 12th International Conference on Applied Geologic Remote Sensing, Denver, Colorado, USA, pp. 91-98.

Kumar, L., K. Schmidt, S. Dury and A. Skidmore, 2001. Imaging spectrometry and vegetation science. In: A. Stein and F. van der Meer (Editor), Imaging Spectrometry. Kluwer Academic Publishers, Netherlands, pp. 111-155.

Lamb, D., M. Steyn-Ross, P. Schaares, M. Hanna, W. Silvester and A. Steyn-Ross, 2002. Estimating leaf nitrogen concentration in ryegrass (Lolium spp.) pasture using the chlorophyll red-edge: theoretical modelling and experimental observations. International Journal of Remote Sensing, 23(18): 3619-3648.

Lillesand, T. and R. Kiefer, 1994. Remote Sensing and Image Interpretation. John Wiley & Sons, Toronto, Canada.

Martin, M., S. Newman, J. Aber and R. Congalton, 1998. Determining forest species composition using high spectral resolution remote sensing data. Remote Sensing of Environment, 65: 249-254.

Martin, M. and J. Aber, 1996. Estimating forest canopy characteristics as inputs for models of forest carbon exchange by high spectral resolution remote sensing. In: H. Gholz, K. Nakane and H. Shimoda (Editor), The Use of Remote Sensing in the Modeling of Forest Productivity. Kluwer Academic Publishing, Dordrecht, The Netherlands, pp. 61-72.

Martin, M. and J. Aber, 1997. High spectral resolution remote sensing of forest canopy lignin, nitrogen, and ecosystem processes. Ecological Applications, 7(2): 431-443.

Matson, P., L. Johnson, C. Billow, J. Miller and P. Rulliang, 1994. Seasonal patterns and remote spectral estimation of canopy chemistry across the Oregon transect. Ecological Applications, 4(2): 280-298.

Moran, J., A. Mitchell, G. Goodmanson and K. Stockburger, 2000. Differentiation among effects of nitrogen fertilization treatments on conifer seedlings by foliar reflectance: a comparison of methods. Tree Physiology, 20: 1113-1120.

Moran, S., D. Hymer, J. Qi and E. Sano, 2000. Soil Moisture evaluation using multi-temporal synthetic aperture radar (SAR) in semiarid rangeland. Agricultural and Forest Meteorology, 105: 69-80.

Mustard, J., 1993. Relationships of soil, grass, and bedrock over the Kaweah serpentine melange through spectral mixture analysis of AVIRIS data. Remote Sensing of Environment, 44: 293-308.

Natural Resources Canada, 2002. Canadian Forest Service: Over a Century of Innovative Solutions.

Niemann, K.O., 1995. Remote sensing of forest stand age using airborne spectrometer data. Photogrammetric Engineering & Remote Sensing, 61(9): 1119-1127.

Ollinger, S., M. Smith, M. Martin, R. Hallett, C. Goodale and J. Aber, 2002. Regional variation in foliar chemistry and soil nitrogen status among forests of diverse history and composition. Ecology, 83: 339-355.

Palacios-Orueta, A. and S. Ustin, 1996. Multivariate statistical classification of soil spectra. Remote Sensing of Environment, 57: 108-118.

Peterson, D., J. Aber, P. Matson, D. Card, N. Swanberg, C. Wessman and M. Spanner, 1988. Remote sensing of forest canopy and leaf biochemical contents. Remote Sensing of Environment, 24: 85-108.

Pierce, L., G. Riggs and S. Running, 1990. Remote detection of canopy water stress in coniferous forests using NS001 Thematic Mapper Simulator and the Thermal Infrared Multispectral Scanner. Photogrammetric Engineering & Remote Sensing, 56: 579-586.

Research Systems Incorporated, 2001. FLAASH User's Guide, The Environment for Visualizing Images (ENVI), Version 3.5.

Riggs, G. and S. Running, 1991. Detection of canopy water stress in conifers using the airborne imaging spectrometer. Remote Sensing of Environment, 35: 51-68.

Sandmeier, S., E. Middleton, D. Deering and W. Qin, 1999. The potential of hyperspectral bidirectional reflectance distribution function data for grass canopy characterization. Journal of Geophysical Research, 104(D8): 9547-9560.

SAS, 2001. What's new in data analysis: Partial Least Squares (PLS). SAS, pp. 2.

Schmidt, K. and A. Skidmore, 2003. Spectral discrimination of vegetation types in a coastal wetland. Remote Sensing of Environment, 85: 92-108.

Secker, J., K. Staenz, P. Budkewitsch and R. Neville, 1999. A vicarious calibration of the Probe-1 hyperspectral sensor, Fourth International Airborne Remote Sensing Conference and Exhibition / 21st Canadian Symposium on Remote Sensing, Ottawa, Ontario, Canada.

Serrano, L., J. Penuelas and S. Ustin, 2002. Remote sensing of nitrogen and lignin in Mediterranean vegetation from AVIRIS data: decomposing biochemical from structural signals. Remote Sensing of Environment, 81: 355-364.

Small, C., 2001. Estimation of urban vegetation abundance by spectral mixture analysis. International Journal of Remote Sensing, 22(7): 1305-1334.

Smith, M., S. Ollinger, M. Martin, J. Aber, R. Hallett and C. Goodale, 2002. Direct estimation of aboveground forest productivity through hyperspectral remote sensing of canopy nitrogen. Ecological Applications, 12(5): 1286-1302.

Smith, M. and M. Martin, 2001. A plot-based method for rapid estimation of forest canopy chemistry. Canadian Journal of Forest Research, 31(3): 549-555.

Stata Corporation, 2003. Stata Statistical Software: Release 8.0, Stata Press.

Thermo Galactic, 2002. Algorithms: Partial Least Squares. www.galactic.com.

van der Meer, F., 1999. Image classification through spectral unmixing. In: A. Stein, F. van der Meer and B. Gorte (Editor), Spatial Statistics for Remote Sensing. Kluwer Academic Publishers, Dordrecht, Netherlands, pp. 185-193.

van der Meer, F., S. de Jong and W. Bakker, 2001. Imaging Spectrometry: Basic Analytical Techniques. In: A. Stein and F. van der Meer (Editor), Imaging Spectrometry. Kluwer Academic Publishers, Dordrecht, Netherlands, pp. 17-61.

Venables, W. and B. Ripley, 1994. Modern Applied Statistics with S-PLUS, Springer-Verlag New York, Incorporated.

Verbyla, D., 1995. Satellite Remote Sensing of Natural Resources. CRC Press, Incorporated, Boca Raton, USA.

Wessman, C., J. Aber, D. Peterson and J. Melillo, 1988. Remote sensing of canopy chemistry and nitrogen cycling in temperate forest ecosystems. Nature, 335: 154-156.

Wessman, C., J. Aber, D. Peterson and J. Melillo, 1988. Foliar analysis using near infrared reflectance spectroscopy. Canadian Journal of Forest Research, 18: 6-11.

Wessman, C., 1990. Evaluation of canopy biochemistry. In: R.a.H.M. Hobbs (Editor), Remote Sensing of Biosphere Functioning. Spinger-Verlag New York, Incorporated, New York.

Wulder, M., E. LeDrew, S. Franklin and M. Lavigne, 1998. Aerial image texture information in the estimation of northern deciduous and mixed wood forest Leaf Area Index (LAI). Remote Sensing of Environment, 64: 64-76.

Yoder, B. and R. Pettigrew-Crosby, 1995. Predicting nitrogen and chlorophyll content and concentrations from reflectance spectra (400-2500 nm) at leaf and canopy scales. Remote Sensing of Environment, 53: 199-211.

APPENDIX A – **Spectral Gain, Offset and Spectral Calibration Files**

Image Channel	Gain
1	500
2	500
3	500
4	500
5	500
6	500
7	500
8	500
9	500
10	500
11	500
12	500
13	500
14	500
15	500
16	500
17	500
18	500
19	500
20	500
21	500
22	500
23	500
24	500
25	500
26	500
27	500
28	500
29	500
30	500
31	500
32	500
33	500
34	500
35	500
36	500
37	500
38	500
39	500
40	500

41	500
42	500
43	500
44	500
45	500
46	500
47	500
48	500
49	500
50	500
51	500
52	500
53	500
54	500
55	500
56	500
57	500
58	500
59	500
60	500
61	500
62	500
63	500
64	500
65	500
66	500
67	500
68	500
69	500
70	500
71	500
72	500
73	500
74	500
75	500
76	500
77	500
78	500
79	500
80	500

81	500
82	500
83	500
84	500
85	500
86	500
87	500
88	500
89	500
90	500
91	500
92	500
93	500
94	500
95	500
96	500
97	500
98	500
99	500
100	500
101	500
102	500
103	500
104	500
105	500
106	500
107	500
108	500
109	500
110	500
111	500
112	500
113	500
114	500
115	500
116	500
117	500
118	500
119	500
120	500

121	500
122	500
123	500
124	500
125	500
126	500
127	500
128	500
129	500
130	500
131	500
132	500
133	500
134	500
135	500
136	500
137	500
138	500
139	500
140	500
141	500
142	500
143	500
144	500
145	500
146	500
147	500
148	500
149	500
150	500
151	500
152	1000
153	1000
154	1000
155	1000
156	1000
157	1000
158	1000
159	1000
160	1000
161	1000
162	1000

163	1000
164	1000
165	1000
166	1000
167	1000
168	1000
169	1000
170	1000
171	1000
172	1000
173	1000
174	1000
175	1000
176	1000
177	1000
178	1000
179	1000
180	1000
181	1000
182	1000
183	1000
184	1000
185	1000
186	1000
187	1000
188	1000
189	1000
190	1000
191	1000
192	1000
193	1000
194	1000
195	1000
196	1000
197	1000
198	1000
199	1000
200	1000
201	1000
202	1000
203	1000
204	1000

Image Channel	Offset
1	0.00
2	0.00
3	0.00
4	0.00
5	0.00
6	0.00
7	0.00
8	0.00
9	0.00
10	0.00
11	0.00
12	0.00
13	0.00
14	0.00
15	0.00
16	0.00
17	0.00
18	0.00
19	0.00
20	0.00
21	0.00
22	0.00
23	0.00
24	0.00
25	0.00
26	0.00
27	0.00
28	0.00
29	0.00
30	0.00
31	0.00
32	0.00
33	0.00
34	0.00
35	0.00
36	0.00
37	0.00
38	0.00
39	0.00
40	0.00
41	0.00
42	0.00
43	0.00
44	0.00
45	0.00
46	0.00
47	0.00
48	0.00
49	0.00
50	0.00
51	0.00
52	0.00
53	0.00
54	0.00
55	0.00
56	0.00
57	0.00
58	0.00
59	0.00
60	0.00
61	0.00
62	0.00
63	0.00
64	0.00
65	0.00
66	0.00
67	0.00
68	0.00
69	0.00
70	0.00
71	0.00
72	0.00
73	0.00
74	0.00
75	0.00
76	0.00
77	0.00
78	0.00
79	0.00
80	0.00
81	0.00
82	0.00
83	0.00
84	0.00
85	0.00
86	0.00
87	0.00
88	0.00
89	0.00
90	0.00
91	0.00
92	0.00
93	0.00
94	0.00
95	0.00
96	0.00
97	0.00
98	0.00
99	0.00
100	0.00
101	0.00
102	0.00
103	0.00
104	0.00
105	0.00
106	0.00
107	0.00
108	0.00
109	0.00
110	0.00
111	0.00
112	0.00
113	0.00
114	0.00
115	0.00
116	0.00
117	0.00
118	0.00
119	0.00
120	0.00
121	0.00
122	0.00
123	0.00
124	0.00
125	0.00
126	0.00
127	0.00
128	0.00
129	0.00
130	0.00
131	0.00
132	0.00

133	0.00
134	0.00
135	0.00
136	0.00
137	0.00
138	0.00
139	0.00
140	0.00
141	0.00
142	0.00
143	0.00
144	0.00
145	0.00
146	0.00
147	0.00
148	0.00
149	0.00
150	0.00
151	0.00
152	0.00
153	0.00
154	0.00
155	0.00
156	0.00
157	0.00
158	0.00
159	0.00
160	0.00
161	0.00
162	0.00
163	0.00
164	0.00
165	0.00
166	0.00
167	0.00
168	0.00
169	0.00
170	0.00
171	0.00
172	0.00
173	0.00

174	0.00
175	0.00
176	0.00
177	0.00
178	0.00
179	0.00
180	0.00
181	0.00
182	0.00
183	0.00
184	0.00
185	0.00
186	0.00
187	0.00
188	0.00
189	0.00
190	0.00
191	0.00
192	0.00
193	0.00
194	0.00
195	0.00
196	0.00
197	0.00
198	0.00
199	0.00
200	0.00
201	0.00
202	0.00
203	0.00
204	0.00

Image Channel	Wavelength	Full-Width-Half-Maximum
1	4.22E+02	1.08E+01
2	4.32E+02	1.06E+01
3	4.42E+02	1.05E+01
4	4.51E+02	1.04E+01
5	4.61E+02	1.03E+01
6	4.71E+02	1.02E+01
7	4.80E+02	1.01E+01
8	4.90E+02	9.99E+00
9	5.00E+02	9.91E+00
10	5.09E+02	9.83E+00
11	5.19E+02	9.77E+00
12	5.29E+02	9.71E+00
13	5.38E+02	9.66E+00
14	5.48E+02	9.62E+00
15	5.58E+02	9.58E+00
16	5.67E+02	9.55E+00
17	5.77E+02	9.53E+00
18	5.87E+02	9.52E+00
19	5.96E+02	9.52E+00
20	6.06E+02	9.52E+00
21	6.16E+02	9.53E+00
22	6.26E+02	9.55E+00
23	6.35E+02	9.57E+00
24	6.45E+02	9.61E+00
25	6.55E+02	9.65E+00
26	6.64E+02	9.70E+00
27	6.74E+02	9.52E+00
28	6.83E+02	9.50E+00
29	6.93E+02	9.48E+00
30	7.02E+02	9.47E+00
31	7.12E+02	9.47E+00
32	7.21E+02	9.48E+00
33	7.31E+02	9.49E+00
34	7.41E+02	9.52E+00
35	7.50E+02	9.55E+00
36	7.60E+02	9.58E+00
37	7.69E+02	9.63E+00
38	7.79E+02	9.68E+00
39	7.88E+02	9.74E+00
40	7.98E+02	9.81E+00
41	8.07E+02	9.89E+00
42	8.17E+02	9.97E+00
43	8.27E+02	1.01E+01
44	8.36E+02	1.02E+01
45	8.46E+02	1.03E+01
46	8.55E+02	1.04E+01
47	8.65E+02	1.05E+01
48	8.75E+02	1.06E+01
49	8.84E+02	1.08E+01
50	8.94E+02	1.09E+01
51	9.03E+02	1.11E+01
52	9.13E+02	1.12E+01
53	9.23E+02	1.14E+01
54	9.31E+02	1.02E+01
55	9.46E+02	9.48E+00
56	9.56E+02	9.47E+00
57	9.65E+02	9.47E+00
58	9.75E+02	9.46E+00
59	9.84E+02	9.45E+00
60	9.94E+02	9.44E+00
61	1.00E+03	9.44E+00
62	1.01E+03	9.43E+00
63	1.02E+03	9.43E+00
64	1.03E+03	9.42E+00
65	1.04E+03	9.42E+00
66	1.05E+03	9.41E+00
67	1.06E+03	9.41E+00
68	1.07E+03	9.64E+00
69	1.08E+03	9.69E+00
70	1.09E+03	9.74E+00
71	1.10E+03	9.41E+00
72	1.11E+03	9.41E+00
73	1.12E+03	9.41E+00
74	1.13E+03	9.41E+00
75	1.14E+03	9.41E+00
76	1.14E+03	9.42E+00
77	1.15E+03	9.42E+00
78	1.16E+03	9.42E+00
79	1.17E+03	9.43E+00
80	1.18E+03	9.43E+00
81	1.19E+03	9.44E+00
82	1.20E+03	9.45E+00
83	1.21E+03	9.45E+00
84	1.22E+03	9.46E+00
85	1.23E+03	9.47E+00
86	1.24E+03	9.48E+00
87	1.25E+03	9.49E+00
88	1.26E+03	1.00E+01

89	1.26E+03	1.11E+01
90	1.27E+03	1.11E+01
91	1.28E+03	1.12E+01
92	1.29E+03	1.12E+01
93	1.30E+03	1.12E+01
94	1.31E+03	1.12E+01
95	1.32E+03	1.12E+01
96	1.33E+03	1.12E+01
97	1.34E+03	1.12E+01
98	1.35E+03	1.12E+01
99	1.36E+03	1.12E+01
100	1.37E+03	1.12E+01
101	1.38E+03	1.12E+01
102	1.39E+03	1.12E+01
103	1.40E+03	1.12E+01
104	1.41E+03	1.12E+01
105	1.42E+03	1.12E+01
106	1.43E+03	1.12E+01
107	1.44E+03	1.12E+01
108	1.45E+03	1.12E+01
109	1.46E+03	1.12E+01
110	1.47E+03	1.12E+01
111	1.48E+03	1.12E+01
112	1.49E+03	1.12E+01
113	1.50E+03	1.12E+01
114	1.51E+03	1.12E+01
115	1.52E+03	1.12E+01
116	1.53E+03	1.12E+01
117	1.54E+03	1.12E+01
118	1.55E+03	1.12E+01
119	1.56E+03	1.12E+01
120	1.57E+03	1.12E+01
121	1.58E+03	1.12E+01
122	1.59E+03	1.11E+01
123	1.60E+03	1.11E+01
124	1.61E+03	1.11E+01
125	1.62E+03	1.11E+01
126	1.63E+03	1.11E+01
127	1.64E+03	1.11E+01
128	1.65E+03	1.10E+01
129	1.66E+03	1.10E+01
130	1.67E+03	1.10E+01
131	1.68E+03	1.10E+01
132	1.69E+03	1.10E+01
133	1.70E+03	1.09E+01
134	1.71E+03	1.09E+01

135	1.72E+03	1.09E+01
136	1.73E+03	1.09E+01
137	1.74E+03	1.09E+01
138	1.75E+03	1.08E+01
139	1.76E+03	1.08E+01
140	1.77E+03	1.08E+01
141	1.78E+03	1.07E+01
142	1.79E+03	1.07E+01
143	1.80E+03	1.07E+01
144	1.81E+03	1.07E+01
145	1.82E+03	1.06E+01
146	1.83E+03	1.06E+01
147	1.84E+03	1.06E+01
148	1.85E+03	1.05E+01
149	1.86E+03	1.05E+01
150	1.87E+03	1.05E+01
151	1.88E+03	1.04E+01
152	1.88E+03	9.90E+00
153	1.89E+03	9.89E+00
154	1.90E+03	9.88E+00
155	1.91E+03	9.86E+00
156	1.92E+03	9.85E+00
157	1.93E+03	9.84E+00
158	1.94E+03	9.83E+00
159	1.95E+03	9.81E+00
160	1.96E+03	9.80E+00
161	1.97E+03	9.79E+00
162	1.98E+03	9.78E+00
163	1.99E+03	9.76E+00
164	2.00E+03	9.75E+00
165	2.01E+03	9.74E+00
166	2.02E+03	9.73E+00
167	2.03E+03	9.72E+00
168	2.04E+03	9.70E+00
169	2.05E+03	9.69E+00
170	2.06E+03	9.68E+00
171	2.07E+03	9.67E+00
172	2.08E+03	9.65E+00
173	2.09E+03	9.64E+00
174	2.10E+03	9.63E+00
175	2.11E+03	9.62E+00
176	2.12E+03	9.61E+00
177	2.13E+03	9.59E+00
178	2.14E+03	9.58E+00
179	2.15E+03	9.57E+00
180	2.16E+03	9.56E+00

181	2.17E+03	9.54E+00
182	2.18E+03	9.53E+00
183	2.19E+03	9.52E+00
184	2.20E+03	9.51E+00
185	2.21E+03	9.49E+00
186	2.22E+03	9.48E+00
187	2.23E+03	9.47E+00
188	2.24E+03	9.46E+00
189	2.25E+03	9.45E+00
190	2.26E+03	9.43E+00
191	2.27E+03	9.42E+00
192	2.28E+03	9.41E+00
193	2.29E+03	9.40E+00
194	2.30E+03	9.38E+00
195	2.31E+03	9.37E+00
196	2.32E+03	9.36E+00
197	2.33E+03	9.35E+00
198	2.34E+03	9.34E+00
199	2.35E+03	9.32E+00
200	2.36E+03	9.31E+00
201	2.37E+03	9.30E+00
202	2.38E+03	9.29E+00
203	2.39E+03	9.28E+00
204	2.40E+03	9.26E+00

APPENDIX B – **AVIRIS Channels and Wavelengths**

Image Channel	AVIRIS Band	Representative Wavelength	Wavelength Range	Full-Width-Half-Maximum
1	6	422.36	427.74 -- 416.98	10.77
2	7	432.03	437.35 -- 426.72	10.63
3	8	441.70	446.96 -- 436.45	10.51
4	9	451.37	456.57 -- 446.18	10.39
5	10	461.04	466.18 -- 455.90	10.28
6	11	470.71	475.80 -- 465.63	10.17
7	12	480.38	485.42 -- 475.34	10.08
8	13	490.05	495.05 -- 485.06	9.99
9	14	499.72	504.68 -- 494.77	9.91
10	15	509.40	514.32 -- 504.49	9.83
11	16	519.07	523.96 -- 514.19	9.77
12	17	528.74	533.60 -- 523.89	9.71
13	18	538.42	543.25 -- 533.59	9.66
14	19	548.09	552.90 -- 543.28	9.62
15	20	557.77	562.56 -- 552.98	9.58
16	21	567.44	572.22 -- 562.67	9.55
17	22	577.12	581.89 -- 572.36	9.53
18	23	586.80	591.56 -- 582.04	9.52
19	24	596.47	601.23 -- 591.71	9.52
20	25	606.15	610.91 -- 601.39	9.52
21	26	615.83	620.60 -- 611.07	9.53
22	27	625.51	630.29 -- 620.74	9.55
23	28	635.19	639.98 -- 630.41	9.57
24	29	644.86	649.67 -- 640.06	9.61
25	30	654.54	659.37 -- 649.72	9.65
26	31	664.26	669.11 -- 659.41	9.70
27	35	673.63	678.39 -- 668.87	9.52
28	36	683.18	687.93 -- 678.43	9.50
29	37	692.72	697.46 -- 687.98	9.48
30	38	702.27	707.01 -- 697.54	9.47
31	39	711.82	716.56 -- 707.09	9.47
32	40	721.38	726.12 -- 716.64	9.48
33	41	730.94	735.69 -- 726.20	9.49
34	42	740.50	745.26 -- 735.74	9.52
35	43	750.06	754.84 -- 745.29	9.55
36	44	759.62	764.41 -- 754.83	9.58
37	45	769.19	774.01 -- 764.38	9.63
38	46	778.76	783.60 -- 773.92	9.68
39	47	788.34	793.21 -- 783.47	9.74
40	48	797.91	802.82 -- 793.01	9.81
41	49	807.49	812.44 -- 802.55	9.89
42	50	817.07	822.06 -- 812.09	9.97
43	51	826.66	831.69 -- 821.63	10.06

44	52	836.25	841.33 -- 831.17	10.16
45	53	845.84	850.98 -- 840.71	10.27
46	54	855.43	860.62 -- 850.24	10.38
47	55	865.02	870.28 -- 859.77	10.51
48	56	874.62	879.94 -- 869.30	10.64
49	57	884.22	889.61 -- 878.84	10.77
50	58	893.83	899.29 -- 888.37	10.92
51	59	903.43	908.97 -- 897.90	11.07
52	60	913.04	918.66 -- 907.43	11.23
53	61	922.65	928.35 -- 916.95	11.40
54	62	930.93	936.03 -- 925.84	10.19
55	63	946.32	951.06 -- 941.58	9.48
56	64	955.78	960.52 -- 951.05	9.47
57	65	965.24	969.98 -- 960.51	9.47
58	66	974.69	979.42 -- 969.96	9.46
59	67	984.15	988.88 -- 979.43	9.45
60	68	993.61	998.33 -- 988.89	9.44
61	69	1003.07	1007.79 -- 998.35	9.44
62	70	1012.53	1017.25 -- 1007.82	9.43
63	71	1021.99	1026.71 -- 1017.28	9.43
64	72	1031.45	1036.16 -- 1026.74	9.42
65	73	1040.90	1045.61 -- 1036.19	9.42
66	74	1050.36	1055.07 -- 1045.66	9.41
67	75	1059.82	1064.53 -- 1055.12	9.41
68	76	1069.35	1074.17 -- 1064.53	9.64
69	77	1078.72	1083.56 -- 1073.87	9.69
70	78	1088.08	1092.95 -- 1083.21	9.74
71	79	1097.65	1102.36 -- 1092.95	9.41
72	80	1107.11	1111.82 -- 1102.41	9.41
73	81	1116.57	1121.28 -- 1111.87	9.41
74	82	1126.03	1130.74 -- 1121.33	9.41
75	83	1135.48	1140.19 -- 1130.78	9.41
76	84	1144.94	1149.65 -- 1140.23	9.42
77	85	1154.40	1159.11 -- 1149.69	9.42
78	86	1163.86	1168.57 -- 1159.15	9.42
79	87	1173.31	1178.03 -- 1168.60	9.43
80	88	1182.77	1187.49 -- 1178.06	9.43
81	89	1192.23	1196.95 -- 1187.51	9.44
82	90	1201.69	1206.42 -- 1196.97	9.45
83	91	1211.14	1215.87 -- 1206.42	9.45
84	92	1220.60	1225.33 -- 1215.87	9.46
85	93	1230.06	1234.80 -- 1225.33	9.47
86	94	1239.51	1244.25 -- 1234.77	9.48
87	95	1248.97	1253.72 -- 1244.23	9.49
88	96	1258.78	1263.80 -- 1253.77	10.03
89	98	1263.47	1269.03 -- 1257.91	11.12
90	99	1273.44	1279.01 -- 1267.87	11.14

91	100	1283.41	1288.99 -- 1277.84	11.15
92	101	1293.37	1298.95 -- 1287.79	11.16
93	102	1303.34	1308.93 -- 1297.76	11.17
94	103	1313.31	1318.90 -- 1307.72	11.18
95	104	1323.28	1328.88 -- 1317.69	11.19
96	105	1333.25	1338.85 -- 1327.65	11.20
97	106	1343.22	1348.83 -- 1337.62	11.21
98	107	1353.19	1358.80 -- 1347.58	11.22
99	108	1363.15	1368.76 -- 1357.54	11.22
100	109	1373.12	1378.74 -- 1367.51	11.23
101	110	1383.09	1388.71 -- 1377.48	11.23
102	111	1393.06	1398.68 -- 1387.44	11.24
103	112	1403.02	1408.64 -- 1397.40	11.24
104	113	1412.99	1418.61 -- 1407.37	11.24
105	114	1422.96	1428.58 -- 1417.34	11.24
106	115	1432.92	1438.54 -- 1427.30	11.24
107	116	1442.89	1448.51 -- 1437.27	11.24
108	117	1452.86	1458.48 -- 1447.24	11.24
109	118	1462.82	1468.44 -- 1457.20	11.24
110	119	1472.79	1478.41 -- 1467.17	11.24
111	120	1482.76	1488.38 -- 1477.15	11.23
112	121	1492.72	1498.34 -- 1487.11	11.23
113	122	1502.69	1508.30 -- 1497.08	11.22
114	123	1512.65	1518.26 -- 1507.04	11.22
115	124	1522.62	1528.23 -- 1517.02	11.21
116	125	1532.58	1538.18 -- 1526.98	11.20
117	126	1542.55	1548.15 -- 1536.96	11.19
118	127	1552.51	1558.10 -- 1546.92	11.18
119	128	1562.48	1568.07 -- 1556.90	11.17
120	129	1572.44	1578.02 -- 1566.86	11.16
121	130	1582.41	1587.99 -- 1576.84	11.15
122	131	1592.37	1597.94 -- 1586.80	11.14
123	132	1602.34	1607.90 -- 1596.78	11.12
124	133	1612.30	1617.86 -- 1606.75	11.11
125	134	1622.27	1627.82 -- 1616.73	11.09
126	135	1632.23	1637.77 -- 1626.69	11.08
127	136	1642.19	1647.72 -- 1636.66	11.06
128	137	1652.16	1657.68 -- 1646.64	11.04
129	138	1662.12	1667.63 -- 1656.61	11.02
130	139	1672.08	1677.59 -- 1666.58	11.01
131	140	1682.05	1687.55 -- 1676.56	10.99
132	141	1692.01	1697.49 -- 1686.53	10.96
133	142	1701.97	1707.44 -- 1696.50	10.94
134	143	1711.93	1717.39 -- 1706.47	10.92
135	144	1721.90	1727.35 -- 1716.45	10.90
136	145	1731.86	1737.30 -- 1726.43	10.87
137	146	1741.82	1747.25 -- 1736.40	10.85

138	147	1751.78	1757.19 -- 1746.37	10.82
139	148	1761.74	1767.14 -- 1756.34	10.80
140	149	1771.70	1777.09 -- 1766.32	10.77
141	150	1781.67	1787.04 -- 1776.30	10.74
142	151	1791.63	1796.99 -- 1786.28	10.71
143	152	1801.59	1806.93 -- 1796.25	10.68
144	153	1811.55	1816.88 -- 1806.23	10.65
145	154	1821.51	1826.82 -- 1816.20	10.62
146	155	1831.47	1836.77 -- 1826.18	10.59
147	156	1841.43	1846.71 -- 1836.16	10.55
148	157	1851.39	1856.65 -- 1846.13	10.52
149	158	1861.35	1866.59 -- 1856.11	10.48
150	159	1871.31	1876.54 -- 1866.09	10.45
151	160	1881.27	1886.48 -- 1876.07	10.41
152	161	1879.34	1884.29 -- 1874.39	9.90
153	162	1889.39	1894.34 -- 1884.45	9.89
154	163	1899.44	1904.38 -- 1894.50	9.88
155	164	1909.49	1914.42 -- 1904.56	9.86
156	165	1919.54	1924.47 -- 1914.62	9.85
157	166	1929.58	1934.50 -- 1924.66	9.84
158	167	1939.62	1944.54 -- 1934.71	9.83
159	168	1949.66	1954.57 -- 1944.76	9.81
160	169	1959.70	1964.60 -- 1954.80	9.80
161	170	1969.73	1974.63 -- 1964.84	9.79
162	171	1979.76	1984.65 -- 1974.87	9.78
163	172	1989.79	1994.67 -- 1984.91	9.76
164	173	1999.81	2004.69 -- 1994.94	9.75
165	174	2009.84	2014.71 -- 2004.97	9.74
166	175	2019.86	2024.73 -- 2015.00	9.73
167	176	2029.88	2034.74 -- 2025.02	9.72
168	177	2039.89	2044.74 -- 2035.04	9.70
169	178	2049.90	2054.75 -- 2045.06	9.69
170	179	2059.91	2064.75 -- 2055.07	9.68
171	180	2069.92	2074.76 -- 2065.09	9.67
172	181	2079.93	2084.76 -- 2075.11	9.65
173	182	2089.93	2094.75 -- 2085.11	9.64
174	183	2099.93	2104.75 -- 2095.12	9.63
175	184	2109.93	2114.74 -- 2105.12	9.62
176	185	2119.92	2124.73 -- 2115.12	9.61
177	186	2129.91	2134.71 -- 2125.12	9.59
178	187	2139.90	2144.69 -- 2135.11	9.58
179	188	2149.89	2154.68 -- 2145.11	9.57
180	189	2159.87	2164.65 -- 2155.09	9.56
181	190	2169.86	2174.63 -- 2165.09	9.54
182	191	2179.83	2184.60 -- 2175.07	9.53
183	192	2189.81	2194.57 -- 2185.05	9.52
184	193	2199.79	2204.55 -- 2195.04	9.51

185	194	2209.76	2214.51 -- 2205.02	9.49
186	195	2219.73	2224.47 -- 2214.99	9.48
187	196	2229.69	2234.43 -- 2224.96	9.47
188	197	2239.66	2244.39 -- 2234.93	9.46
189	198	2249.62	2254.35 -- 2244.90	9.45
190	199	2259.58	2264.30 -- 2254.87	9.43
191	200	2269.53	2274.24 -- 2264.82	9.42
192	201	2279.49	2284.20 -- 2274.79	9.41
193	202	2289.44	2294.14 -- 2284.74	9.40
194	203	2299.38	2304.07 -- 2294.69	9.38
195	204	2309.33	2314.02 -- 2304.65	9.37
196	205	2319.27	2323.95 -- 2314.59	9.36
197	206	2329.21	2333.89 -- 2324.54	9.35
198	207	2339.15	2343.82 -- 2334.48	9.34
199	208	2349.09	2353.75 -- 2344.43	9.32
200	209	2359.02	2363.68 -- 2354.37	9.31
201	210	2368.95	2373.60 -- 2364.30	9.30
202	211	2378.88	2383.53 -- 2374.24	9.29
203	212	2388.80	2393.44 -- 2384.16	9.28
204	213	2398.73	2403.36 -- 2394.10	9.26

APPENDIX C – **SAS Regression Script**

```
/* library name*/
libname Bioind '';

/* set output ODS file*/
ods output Xloadings=xloadings;

/* parameters for PLS regression */
proc pls data=Bioind.df_chemistry
        method=pls
        nfac=15
        cv=one
        details;

        model chemical_m = A_CHAN1_LAM422_36 A_CHAN2_LAM432_03
            A_CHAN3_LAM441_7 A_CHAN4_LAM451_37 A_CHAN5_LAM461_04
            A_CHAN6_LAM470_71 A_CHAN7_LAM480_38 A_CHAN8_LAM490_05
            A_CHAN9_LAM499_72 A_CHAN10_LAM509_4 A_CHAN11_LAM519_07
            A_CHAN12_LAM528_74 A_CHAN13_LAM538_42 A_CHAN14_LAM548_09
            A_CHAN15_LAM557_77 A_CHAN16_LAM567_44 A_CHAN17_LAM577_12
            A_CHAN18_LAM586_8 A_CHAN19_LAM596_47 A_CHAN20_LAM606_15
            A_CHAN21_LAM615_83 A_CHAN22_LAM625_51 A_CHAN23_LAM635_19
            A_CHAN24_LAM644_86 A_CHAN25_LAM654_54 A_CHAN26_LAM664_26
            A_CHAN27_LAM673_63 A_CHAN28_LAM683_18 A_CHAN29_LAM692_72
            A_CHAN30_LAM702_27 A_CHAN31_LAM711_82 A_CHAN32_LAM721_38
            A_CHAN33_LAM730_94 A_CHAN34_LAM740_5 A_CHAN35_LAM750_06
            A_CHAN36_LAM759_62 A_CHAN37_LAM769_19 A_CHAN38_LAM778_76
            A_CHAN39_LAM788_34 A_CHAN40_LAM797_91 A_CHAN41_LAM807_49
            A_CHAN42_LAM817_07 A_CHAN43_LAM826_66 A_CHAN44_LAM836_25
            A_CHAN45_LAM845_84 A_CHAN46_LAM855_43 A_CHAN47_LAM865_02
            A_CHAN48_LAM874_62 A_CHAN49_LAM884_22 A_CHAN50_LAM893_83
            A_CHAN51_LAM903_43 A_CHAN52_LAM913_04 A_CHAN53_LAM922_65
            A_CHAN54_LAM930_93 A_CHAN55_LAM946_32 A_CHAN56_LAM955_78
            A_CHAN57_LAM965_24 A_CHAN58_LAM974_69 A_CHAN59_LAM984_15
            A_CHAN60_LAM993_61 A_CHAN61_LAM1003_07 A_CHAN62_LAM1012_53
            A_CHAN63_LAM1021_99 A_CHAN64_LAM1031_45 A_CHAN65_LAM1040_9
            A_CHAN66_LAM1050_36 A_CHAN67_LAM1059_82 A_CHAN68_LAM1069_35
            A_CHAN70_LAM1088_08 A_CHAN71_LAM1097_65 A_CHAN72_LAM1107_11
            A_CHAN73_LAM1116_57 A_CHAN74_LAM1126_03 A_CHAN75_LAM1135_48
            A_CHAN76_LAM1144_94 A_CHAN77_LAM1154_4 A_CHAN78_LAM1163_86
            A_CHAN79_LAM1173_31 A_CHAN80_LAM1182_77 A_CHAN81_LAM1192_23
            A_CHAN82_LAM1201_69 A_CHAN83_LAM1211_14 A_CHAN84_LAM1220_6
            A_CHAN85_LAM1230_06 A_CHAN86_LAM1239_51 A_CHAN87_LAM1248_97
            A_CHAN88_LAM1258_78 A_CHAN89_LAM1263_47 A_CHAN90_LAM1273_44
            A_CHAN91_LAM1283_41 A_CHAN92_LAM1293_37 A_CHAN93_LAM1303_34
            A_CHAN94_LAM1313_31 A_CHAN95_LAM1323_28 A_CHAN96_LAM1333_25
            A_CHAN97_LAM1343_22 A_CHAN106_LAM1432_92 A_CHAN107_LAM1442_89
            A_CHAN108_LAM1452_86 A_CHAN109_LAM1462_82 A_CHAN110_LAM1472_79
            A_CHAN111_LAM1482_76 A_CHAN112_LAM1492_72 A_CHAN113_LAM1502_69
            A_CHAN114_LAM1512_65 A_CHAN115_LAM1522_62 A_CHAN116_LAM1532_58
            A_CHAN117_LAM1542_55 A_CHAN118_LAM1552_51 A_CHAN119_LAM1562_48
            A_CHAN120_LAM1572_44 A_CHAN121_LAM1582_41 A_CHAN122_LAM1592_37
            A_CHAN123_LAM1602_34 A_CHAN124_LAM1612_3 A_CHAN125_LAM1622_27
            A_CHAN126_LAM1632_23 A_CHAN127_LAM1642_19 A_CHAN128_LAM1652_16
            A_CHAN129_LAM1662_12 A_CHAN130_LAM1672_08 A_CHAN131_LAM1682_05
            A_CHAN132_LAM1692_01 A_CHAN133_LAM1701_97 A_CHAN134_LAM1711_93
            A_CHAN135_LAM1721_9 A_CHAN136_LAM1731_86 A_CHAN137_LAM1741_82
```

```
A_CHAN138_LAM1751_78 A_CHAN139_LAM1761_74 A_CHAN140_LAM1771_7
A_CHAN141_LAM1781_67 A_CHAN142_LAM1791_63 A_CHAN143_LAM1801_59
A_CHAN159_LAM1949_66 A_CHAN160_LAM1959_7 A_CHAN161_LAM1969_73
A_CHAN162_LAM1979_76 A_CHAN163_LAM1989_79 A_CHAN164_LAM1999_81
A_CHAN165_LAM2009_84 A_CHAN166_LAM2019_86 A_CHAN167_LAM2029_88
A_CHAN168_LAM2039_89 A_CHAN169_LAM2049_9 A_CHAN170_LAM2059_91
A_CHAN171_LAM2069_92 A_CHAN172_LAM2079_93 A_CHAN173_LAM2089_93
A_CHAN174_LAM2099_93 A_CHAN175_LAM2109_93 A_CHAN176_LAM2119_92
A_CHAN177_LAM2129_91 A_CHAN178_LAM2139_9 A_CHAN179_LAM2149_89
A_CHAN180_LAM2159_87 A_CHAN181_LAM2169_86 A_CHAN182_LAM2179_83
A_CHAN183_LAM2189_81 A_CHAN184_LAM2199_79 A_CHAN185_LAM2209_76
A_CHAN186_LAM2219_73 A_CHAN187_LAM2229_69 A_CHAN188_LAM2239_66
A_CHAN189_LAM2249_62 A_CHAN190_LAM2259_58 A_CHAN191_LAM2269_53
A_CHAN192_LAM2279_49 A_CHAN193_LAM2289_44 A_CHAN194_LAM2299_38
A_CHAN195_LAM2309_33 A_CHAN196_LAM2319_27 A_CHAN197_LAM2329_21
A_CHAN198_LAM2339_15 A_CHAN199_LAM2349_09 A_CHAN200_LAM2359_02
A_CHAN201_LAM2368_95 A_CHAN202_LAM2378_88 A_CHAN203_LAM2388_8
A_CHAN204_LAM2398_73;

output out = chemical_m_pls predicted = predict yresidual = yres1 xresidual = xres1-xres181
  xscore = xscore yscore = yscore
                    h = h press = press xqres = xqres yqres = yqres / INTERCEPT SOLUTION;
run;

/* create xloadings temporary output file*/
ods listing;
proc transpose data = xloadings (drop = NumberofFactors)
        out = xloadings;

data xloadings;
 set xloadings;
   n = _n_;
   rename col1-col20 = factor1-factor20;

run;
quit;
```

APPENDIX D – **EASI Derivatives Script**

```
!  Revised by M. Murdoch,  February 12, 2003
!  Revised by L. Cai        February 28, 2003
!  Revised by J. Ryall  July 16, 2003
!  Fixed the formula of calculating derivatives by using Crammer's Rule
DOC        DERIV
DOC
DOC This script computes the derivative of an image by looking at
DOC  surrounding bands.
DOC The derivative at any band is taken by using the surrounding bands'
DOC wavelength as the input [X] matrix and the values of each pixel as
DOC the [Y] matrix. Using Crammer's Rule, DERIV calculates the
DOC coefficients of the parabola passing through the 3
DOC points defines by the (band wavelength, value) points. The
DOC derivative is calculated based
DOC on:
DOC     2ax + b
DOC
DOC Where a and b are the parabola's coefficients calculated by
DOC Crammer's Rule.
DOC
DOC The second derivative is calculated and output as an additional
DOC file.
DOC
DOC The resulting image will be in units 100*(a / nm), where a = the "y"
DOC unit of the
DOC input image (ex. reflectance (%)) because of the high spread of
DOC numbers in the output,
DOC accuracy is limited to approximately 2 decimal places.
DOC
DOC 1 Parameters
DOC @verbatim
DOC Name     Prompt                    Count        Type
DOC
DOC FILI     Input File                1-64         Char
DOC FILO     Output File               0-64         Char
DOC STR1     Sensor Type               1-64         Char
DOC
DOC @end
DOC
DOC 2 FILI
DOC The FILI parameter is a PCIDSK input file.
DOC
DOC FILI = "d1s1_atm_geo_forcefit.pix"
DOC
DOC 2 FILO
DOC FILO is an optional parameter.  DERIV by default will create an
output file
DOC with _deriv.pix appended to the same filename as FILI.
DOC
DOC 2 STR1
DOC
DOC This parameter specifies the sensor type, which will determine the
DOC function
DOC in HYP_LIB which is called to get the wavelengths.
DOC
DOC Currently the following data types are supported:
DOC STR1 = "av01"    -->  AVIRIS 2001
```

```
DOC      = "av02"   -->  AVIRIS 2002
DOC
DOC 1 Version
DOC @verbatim
DOC v1.00 20021230 AFT PFC CFS NRCan CA
DOC
DOC v1.01 20030211 M. Murdoch AFT PFC CFS NRCan CA
DOC
DOC v1.1  20030228 L. Cai AFT PFC CFS NRCan CA
DOC
DOC v1.2  20030716 J. Ryall AFT PFC CFS NRCan CA
DOC       - simplified formula for first and second derivatives
DOC       - added ability to process both AVIRIS 2001 and AVIRIS 2002
DOC         data
DOC
DOC @end

STATUS_TITLE "DERIV - Calculates Derivative"
STATUS_SHOW FILI 64,1
STATUS_SHOW FILO 64,0
STATUS_SHOW STR1 64,1

!*****************************************************************************
!
!                              Start Main Program
!
!*****************************************************************************
!
!-----------------------------------------------------------------------------
!
!                         Load HYP_LIB                                      !
! - Uses AVIRISwavelength()                                                 !
!-----------------------------------------------------------------------------
!
LOAD "HYP_LIB"
!-----------------------------------------------------------------------------
!
!                               Local Variables
!
!-----------------------------------------------------------------------------
!
LOCAL integer finid, foutid, foutid2
LOCAL string fin, fout1, fout2
LOCAL integer numChannels
LOCAL integer counter, i, j
LOCAL mstring wavefile, wtokens
LOCAL int maxChannel, chancount
LOCAL string chanDescription, oldChanDescription
LOCAL GeoInfo gi
LOCAL integer deriv_flag

!-----------------------------------------------------------------------------
!
!                              Initialize Variables
!
!-----------------------------------------------------------------------------
!
```

```
counter = 0
i = 0
j = 0
chancount = 0

!-------------------------------------------------------------------------
!
!                    Check Input Parameters
!
!-------------------------------------------------------------------------
!
fin = fili
if F$Extract( GetStat( fin ), 1, 1 ) != "F" then
    printf "DERIV ERROR: Input file \"%s\" does not exist\n",\
           fin
    RETURN
endif

fout1 = filo

if (fout1 = "") then
    fout1 = F$EXTRACT(fin, 1, F$LEN(fin)-4) + "_deriv.pix"
    fout2 = F$EXTRACT(fin, 1, F$LEN(fin)-4) + "_2nd_deriv.pix"
else
    fout2 = F$EXTRACT(filo, 1, F$LEN(filo)-4) + "_2nd_deriv.pix"
endif

!-------------------------------------------------------------------------
!
!                     Open Files
!
!-------------------------------------------------------------------------
!
finid = DBOpen(fin, "r")
foutid = DBOpen(fout1, "r")
foutid2 = DBOpen(fout2, "r")

! Save number of channels
numChannels = DBChannels(fili)

! Define array of wavelengths of size numChannels
LOCAL double wavelength[numChannels]

foutid = DBCreate( fout1, "PIX", DBPixels(finid), DBLines(finid), \
                   DBChannels(finid), "32R", "" )

CALL DBReadGeoInfo( finid, gi )
CALL DBWriteGeoInfo( foutid, gi )

foutid2 = DBCreate( fout2, "PIX", DBPixels(finid), DBLines(finid), \
                   DBChannels(finid), "32R", "" )

CALL DBReadGeoInfo( finid, gi )
CALL DBWriteGeoInfo( foutid2, gi )

!-------------------------------------------------------------------------
!
```

```
! Using wavelength values to include horizontal aspect of points in
! calculation.
!-------------------------------------------------------------------------
!
! Calls HYP_LIB.EAS
if (STR1 = "av01") then
   wavefile = AVIRIS01wavelength( )
elseif (STR1 = "av02") then
   wavefile = AVIRIS02wavelength( )
else
   printf "DERIV FLAG: Unable to determine sensor."
   stop
endif

!wavefile = AVIRIS01wavelength( )

for i = 1 to F$LEN(wavefile)
     if ( i = 1 ) then
         wtokens = tokenize(wavefile[i],"{")
       wtokens = tokenize(wtokens[2],",")
     elseif ( i = F$LEN(wavefile) ) then
         wtokens = tokenize(wavefile[i],"}")
       wtokens = tokenize(wtokens[1],",")
     else
         wtokens = tokenize(wavefile[i],",")
     endif

     for j = 1 to F$LEN(wtokens)
         chancount = chancount +1
       if ( chancount <= numChannels ) then
           wavelength[chancount] = F$VALUE(wtokens[j])
!          printf "%i   wavelength = %f\n", chancount,
wavelength[chancount]
         endif
     endfor
endfor

! Look at the difference of the wavelength, there shouldn't be negative
values
!for i =2 to F$LEN(wavelength)
!    print i, ": ", wavelength [i], " ", b-a
!endfor

!-------------------------------------------------------------------------
!
! Calculates the derivative at each channel and stores in output file.
!
! Note that the method uses surrounding bands, so the first and last
!
! bands of the image have no defined derivative.
!
!-------------------------------------------------------------------------
!
printf "Calculating the derivative.........\n"
model on FOUT1

    maxChannel = numChannels-1
```

```
    %1 = 0
    %{numChannels} = 0

    LOCAL int k
    LOCAL double a, b, c, calc

    for k=2 to maxChannel

       !These values change each time the loop begins again
       a = wavelength[k-1]
       b = wavelength[k]
       c = wavelength[k+1]

       calc = b*a*a + a*c*c + c*b*b - a*b*b - c*a*a - b*c*c
       %{k}=( 2*(  b* ( %{finid,k-1} - %{finid,k+1} ) + \
                  a* ( %{finid,k+1} - %{finid,k} ) + \
                c* ( %{finid,k} - %{finid,k-1} )) / calc*b + \
                 (a*a* ( %{finid,k} - %{finid,k+1} ) + \
              c*c* ( %{finid,k-1} - %{finid,k} ) + \
                b*b* ( %{finid,k+1} - %{finid,k-1} ) ) / calc)
       oldChanDescription = DBReadChanDesc(finid, k)
       chanDescription = oldChanDescription + " - Derivative"
       CALL DBWriteChanDesc(foutid, k, chanDescription)
    endfor
endmodel

printf "Calculating the 2nd derivative.....\n"
model on FOUT2

   maxChannel = numChannels-1
   %1 = 0
   %{numChannels} = 0

    LOCAL int m
    LOCAL double a, b, c, calc

    for m=2 to maxChannel

       !These values change each time the loop begins again
       a = wavelength[m-1]
       b = wavelength[m]
       c = wavelength[m+1]

       calc = b*a*a + a*c*c + c*b*b - a*b*b - c*a*a - b*c*c

          %{m}=(2*(%{finid,m-1}*b + %{finid,m+1}*a + \
             %{finid,m}*c - %{finid,m}*a - c*%{finid,m-1} - \
             %{finid,m+1}*b)/ calc)
          oldChanDescription = DBReadChanDesc(finid, m)
          chanDescription = oldChanDescription + " - 2nd Derivative"
          CALL DBWriteChanDesc(foutid2, m, chanDescription)

    endfor
endmodel


call DBClose(finid)
```

```
call DBClose(foutid)
call DBClose(foutid2)

RETURN
```

APPENDIX E – **EASI Mapping Script**

```
! Written by M. Murdoch, April 23, 2003
DOC PLSREG
DOC
DOC PLSREG applies regression coefficients to image file specified by
DOC the users. Note that if the regression coefficients are ran on a
DOC reflectance file the values must be scaled by 10000 to convert to
DOC true reflectance. This can be done in this script by removing the
DOC exclamation mark on line 127.
DOC
DOC 1 Parameters
DOC
DOC 2 FILE
DOC
DOC FILE = "2001_atm_geo_ff_absorb_ss.pix"
DOC
DOC 2 TFILE
DOC TFILE is a file containing the regression coefficients.
DOC
DOC TFILE = "coefficients.txt"
DOC
DOC The text file can only contain one column, which contains the
DOC regression coefficients. The first entry in that column must the
DOC offset, following by a regression coefficient for each band.  The
DOC number of regression coefficients must equal the number of bands.
DOC
DOC @verbatim
DOC      0.05345353       - This would be the offset
DOC      -0.34535345      - First regression coefficient
DOC      0.342342432      - Second regression coefficient
DOC @end
DOC 1 Version
DOC @verbatim
DOC v1.00 20030423 M. Murdoch AFT PFC CFS NRCan CA
DOC v1.01 20030620 A. Dyk AFT PFC CFS NRCan CA - Fixed formula Errors
DOC and clean up code. Added Filter
DOC @end

STATUS_TITLE "PLSREG - Applies Regression Coefficients from PLS."
STATUS_SHOW FILE
STATUS_SHOW TFILE
STATUS_SHOW FLSZ 2, 2

!*****************************************************************!
!                           Start Main Program
!
!*****************************************************************!

!-----------------------------------------------------------------!
!                           Local Variables                       !
!-----------------------------------------------------------------!
LOCAL integer finid, foutid, filtersize
LOCAL string fin, fout
LOCAL integer numChannels
LOCAL integer i
LOCAL string textfile
LOCAL mstring regression_coeff, wtokens
LOCAL GeoInfo gi
```

```
!-------------------------------------------------------------------------!
!                      Check Input Parameters
!-------------------------------------------------------------------------!
fin = file
if F$Extract( GetStat( fin ), 1, 1 ) != "F" then
    printf "PLSREG ERROR: Input file \"%s\" does not exist\n",\
           fin
    RETURN
endif

textfile = tfile
if F$Extract( GetStat( textfile ), 1, 1 ) != "F" then
    printf "PLSREG ERROR: Input file \"%s\" does not exist\n",\
           textfile
    RETURN
endif

fout = GetFileBaseName( fin ) + "_reg.pix"
! F$EXTRACT( fin, 1, F$LEN( fin )-4 ) + "_reg.pix" \! Code changed

filtersize = FLSZ(1)

!-------------------------------------------------------------------------!
!                     Open Files                                          !
!-------------------------------------------------------------------------!
finid = DBOpen( fin, "r" )
if F$Extract( GetStat( fout ), 1, 1 ) = "F" then
   printf "PLSREG WARNING: \"%s\" already exists, replacing!\n", fout
   DEL fout
endif

foutid = DBCreate( fout, "PIX", DBPixels( finid ), \
                   DBLines( finid ), 1, "32R", "" )

CALL DBReadGeoInfo( finid, gi )
CALL DBWriteGeoInfo( foutid, gi )

!-------------------------------------------------------------------------!
! Read in load factors for TFILE and store then in two array's
!
!-------------------------------------------------------------------------!
regression_coeff = Text$Import( textfile )
numChannels = F$LEN( regression_coeff )  \! include the intercept

if ( numChannels - 1 <> ( DBChannels( finid ) ) ) then
    printf "PLSREG ERROR: \"%s\" has wrong number of channels\n", TFILE
    printf "FLAG: TFILE's numchannnels = %d, \"%s\" Number of Channels =
%d\n", numChannels, fin, DBChannels( finid )
    RETURN
endif

! LOCAL integer Chan[ numChannels ]
LOCAL float regcoeff[ numChannels ]

for i = 1 to numChannels
   regcoeff[ i ] = F$VALUE( regression_coeff[ i ] )
if (i = 1) then
```

```
   printf "%3d - Intercept = %f\n", i - 1, regcoeff[ i ]
else
   printf "%3d - Chan %3d = %f\n", i, i - 1, regcoeff[ i ]
endif

endfor

!-------------------------------------------------------------------------!
!                    Applies Load Factors                                 !
!-------------------------------------------------------------------------!
printf "Applying Regression Coefficients.....\n"
model on FOUT
    local integer i
    %{ foutid, 1 } = regcoeff[ 1 ]  \! intercept
    for i = 2 to numChannels
        %{ foutid, 1 } = %{ foutid, 1 } + \
      ( %{ finid, i - 1 } / 10000 * regcoeff[ i ] )
    endfor
!    printf "%7f\n", %{foutid, 1}
!    %{foutid,1} = (%{foutid,1}/10000)
endmodel

!-------------------------------------------------------------------------!
!        Filter Results if FLSZ > 1X1
!-------------------------------------------------------------------------!

if ( Filtersize > 1 ) then
   FILE = fout
   DBIC = 1
   DBOC = 1
   MASK =
   FLSZ = filtersize, filtersize
   printf "PLSREG FLAG: Filtering results with %dX%d\n", \
           filtersize, filtersize
   R FAV
else

endif

!-------------------------------------------------------------------------!
!        Close Files                                          !
!-------------------------------------------------------------------------!

call DBClose( finid )
call DBClose( foutid )

!-------------------------------------------------------------------------!
!        Finishing remarks
!-------------------------------------------------------------------------!

printf "PLSREG FLAG: All Done, Please see \"%s\" for output\n", fout
RETURN
```